

Sveinung T. Karlsen, Jakob B. Kristiansen, Stewart
G. Robertson

Accuracy of Tilt-compensated GNSS- sensors using Network-RTK

Bacheloroppgåve i Geomatikk

Rettleiar: Tormod Urke

Mai 2021

Sveinung T. Karlsen, Jakob B. Kristiansen, Stewart G. Robertson

Accuracy of Tilt-compensated GNSS-sensors using Network-RTK

Bacheloroppgåve i Geomatikk
Rettleiar: Tormod Urke
Mai 2021

Noregs teknisk-naturvitskaplege universitet
Fakultet for ingeniørvitenskap
Institutt for vareproduksjon og byggingsteknikk





Kunnskap for en bedre verden

Accuracy of Tilt-compensated GNSS-sensors using Network-RTK

Sveinung T. Karlsen, Jakob B. Kristiansen & Stewart G. Robertson

Gradering: Åpen

Bachelor i ingeniørfag - geomatikk

Innlevert: Mai 2021

Veileder: Tormod Urke

Norges teknisk-naturvitenskapelige universitet
Institutt for vareproduksjon og byggingsteknikk

| | | | |
|--|--------------------------|-----------------|---|
| Oppgavens tittel: Accuracy of Tilt-compensated GNSS-sensors using Network-RTK | Dato: 19.05.21 | | |
| | Antall sider: 57 [sider] | | |
| | Masteroppgave: | Bacheloroppgave | X |
| Navn: Sveinung Tangen Karlsen, Jakob Brysting Kristiansen, Stewart George Robertson | | | |
| Veileder: Tormod Urke | | | |

Samandrag:

GNSS-sensorar er ein sentral del av fagområdet geomatikk, problemet er ofte vatring eller punkt som ein ikkje kan vere direkte over. I denne oppgåva nyttar vi to ulike sensorar for å finne ut av kor mykje nytte ein får ut av tilt-teknologien som er tilgjengeleg i dag.

Det er sett opp fire ulike metodar der ein kan sjå på nytteverdien av teknologien. Vi gjennomførte to testar i ideelle forhold med ulike grader av tilt med begge sensorane og tilting mot forskjellige himmelretningar med maks utslag av tilt. Det var også gjennomførte hushjørne innmålingar som er vanleg i landsmålingssamanheng, samt måling i kum.

Teorien inkludert tidlegare studia blir gjennomgått og kopla opp mot resultatata for dei ulike metodane. Resultata visar varierende grad overbestemmelse med instrumentleverandørane sine teknisk spesifikasjonar.

Sensor A hadde opptil 23 cm i grunnriss og sensor B hadde inntil 4 cm i grunnriss for metode 1 og 2. Presisjonen til sensor A var som forventa, dog ikkje nøyaktigheita. Sensor B følgjer tilnærma lik produsenten sine tekniske spesifikasjonar for metode 1 og 2.

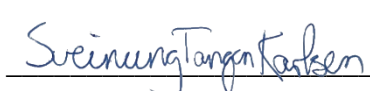
Bruk av sensorane i krevjande målemiljø tilsa nedsatt nøyaktigheit. Nøyaktigheita for innmåling av hushjørner og vann- og avløpssystemer i metode 3 og 4 var hovudsakleg innanfor krava til dei relevante standardane.

Stikkord:

| |
|-------------------|
| GNSS |
| Tilt-compensation |
| Surveying |
| Geomatics |



Jakob Kristiansen



Sveinung Tangen Karlsen



Stewart Robertson

Abstract

In this thesis, tilt-compensated GNSS-sensors are tested and analysed through four different methods on the campus of NTNU Gjøvik. The ability to measure points that cannot be measured with conventional GNSS-sensors increases the areas of use and efficiency if the accuracy is suitable. Two separate receivers are chosen, known as receiver A and receiver B.

There are four different methods where we observe the effects of the process. The first method involves observations at varying degrees of tilt with the same attitude, to see how the observations behave at varying degrees of tilt. Method two has the sensor tilted towards the four cardinal directions to look for bias. Method three is a realistic situation of measuring building corners. The fourth method is measuring a pipe in a manhole, which also is not possible with conventional GNSS equipment.

The theory and earlier studies are presented and connected to the results of the different methods. Results show how the completed observations vary within the datasets and give a basis for the discussion.

Receiver A had a horizontal accuracy of up to 23 cm for method 1 and 2. The precision of receiver A and the accuracy of height was within the expected range, the accuracy of the horizontal plane was not. Receiver B roughly follows the expected precision and accuracy of the producer. The accuracy requirements are met for buildings with an accuracy of 2-4 cm. Sewage and waterways have the strictest requirements of 3 cm along the horizontal plane, these are predominantly met.

Preface

This bachelor's thesis is our final report for the Bachelor Geomatic's course at NTNU Gjøvik, Department of Manufacturing and Civil Engineering.

The project was initially selected due to our interest in the new equipment the university acquired, GNSS receivers with tilt compensation. Researching the literature revealed how few studies there were pertaining to equipment reliability save for the producers' own studies.

Thank you to our supervisor Tormod Urke for his help and for being available as someone we could bounce ideas off of and for feedback during the process. An extra big thanks to both the receivers' producers for lending us the equipment, making this thesis possible. We also want to thank Morten Eggum for always being helpful with our questions and arranging equipment.

In addition, a big thanks to all our friends and fellow students for some excellent discussions, both professional and unprofessional.

And lastly a big thanks to our friends and family for supporting us through these 3 years.

Table of Contents

| | |
|--|-----|
| Abstract..... | i |
| Preface..... | ii |
| Figure & table list | v |
| Abbreviations & terms..... | vii |
| 1 Introduction..... | 1 |
| 1.1 Background | 1 |
| 1.2 Purpose..... | 1 |
| 1.3 Limitations | 2 |
| 1.4 United Nations - Sustainable Development Goals..... | 2 |
| 2 Theory | 3 |
| 2.1 Static measurements..... | 3 |
| 2.2 Network RTK..... | 3 |
| 2.3 Hardware | 4 |
| 2.3.1 Receiver A | 4 |
| 2.3.2 Receiver B | 4 |
| 2.3.4 IMU and INS | 5 |
| 2.4 Sources of error | 6 |
| 2.5 Aspects of Data-processing..... | 6 |
| 2.6 Previous studies..... | 8 |
| 3 Method..... | 11 |
| 3.1 Reference points..... | 11 |
| 3.2 Method 1 – Tilt-compensation at varying degrees..... | 13 |
| 3.3 Method 2 – Visible satellite bias for cardinal directions..... | 14 |
| 3.4 Method 3 – Measuring building corners | 15 |
| 3.5 Method 4 - Manhole..... | 16 |
| 4 Results..... | 17 |

| | |
|---|----|
| 4.1 Reference points | 17 |
| 4.2 Method 1 – Tilt-compensation of varying degrees | 17 |
| 4.2.1 Receiver A | 17 |
| 4.2.2 Receiver B | 22 |
| 4.3 Method 2 – Cardinal directions | 24 |
| 4.3.1 Receiver A | 24 |
| 4.3.2 Receiver B | 27 |
| 4.4 Method 3 – Building corners..... | 30 |
| 4.4.2 Receiver A | 30 |
| 4.4.3 Receiver B | 32 |
| 4.5 Method 4 – Manhole | 34 |
| 5 Discussion | 36 |
| 5.1 Considerations | 36 |
| 5.2 Observation results..... | 37 |
| 5.2.1 M1 Varying degrees of tilt..... | 37 |
| 5.2.2 M2 Cardinal directions..... | 38 |
| 5.2.3 M3 Building corners..... | 39 |
| 5.2.4 M4 Manhole | 39 |
| 6 Conclusion and future studies..... | 41 |
| 6.1 Conclusion..... | 41 |
| 6.2 Future studies | 42 |
| References..... | 43 |
| Appendix..... | 47 |

Figure & table list

| | |
|--|----|
| TABLE 1 - PRODUCERS HORIZONTAL STATED ACCURACY FOR LEVELLED RTK (L1+L2) AND COMPENSATOR TILT SENSOR UNCERTAINTY. | 4 |
| TABLE 2 - PRODUCERS HORIZONTAL STATED ACCURACY FOR LEVELLED RTK(L1/L2), AND COMPENSATOR TILT SENSOR UNCERTAINTY. | 5 |
| FIGURE 1 - VARIABLES FOR ESTIMATING DISTANCE FROM ANTENNA RECEIVER TO REFERENCE POINT IN THE GROUND PLANE. (FIGURE: SVEINUNG KARLSEN, 2021). | 8 |
| FIGURE 2 - MAP SNIPPET COLLECTED FROM NORGESKART.NO VISUALIZING BASE STATIONS DISTANCE IN ADDITION TO WHERE MOST OF THE OBSERVATIONS TOOK PLACE (RED TRIANGLE)..... | 11 |
| FIGURE 3 - T1 AND P1 (PHOTO: JAKOB B KRISTIANSEN, 2021) | 12 |
| FIGURE 4 -THE G BUILDING. T1 WAS ESTABLISHED ON THE BALCONY ON THE LOWER ROOF. (PHOTO: JAKOB B KRISTIANSEN, 2021)..... | 12 |
| FIGURE 5 - MODEL OF M1 IN PRACTICE. (FIGURE: SVEINUNG KARLSEN, 2021). | 13 |
| FIGURE 6 - MODEL OF M2 IN PRACTICE. (FIGURE: SVEINUNG KARLSEN, 2021). | 14 |
| FIGURE 7 - BUILDING CORNERS WITH APPROXIMATE DIRECTION OF TILT INDICATED BY THE ARROWS..... | 15 |
| FIGURE 8 - THE H AND S BUILDINGS (PHOTO: JAKOB B KRISTIANSEN, 2021) | 15 |
| FIGURE 9 - MANHOLE, THE POINT THAT WAS MEASURED WAS ON TOP OF THE PIPE. (PHOTO: SVEINUNG KARLSEN, 2021)..... | 16 |
| TABLE 3 - REFERENCE POINTS COORDINATE AFTER THE ADJUSTMENT CALCULATION IN ADDITION TO STANDARD DEVIATION (U). | 17 |
| TABLE 4 - M1A STANDARD DEVIATION AND AVERAGE SIZE OF DEVIATION (D) FROM BENCHMARK T1 (U) FOR NORTHING(N), EASTING(E), HEIGHT(H), RMS FOR THE HORIZONTAL PLANE(2D) AND RA. | 18 |
| FIGURE 10 - M1A STANDARD DEVIATION OF OBSERVATIONS. | 18 |
| FIGURE 11 – M1A AVERAGE DEVIATION FROM T1..... | 19 |
| FIGURE 12 - M1A SCATTERPLOT OF THE DEVIATIONS OF OBSERVATIONS FROM THE BENCHMARK T1..... | 20 |
| TABLE 5 - RATIO BETWEEN T1 AND DISTANCE TO THE RECEIVER ALONG THE HORIZONTAL PLANE..... | 20 |
| TABLE 6 - M1B STANDARD DEVIATION AND AVERAGE SIZE OF DEVIATION (D) FROM BENCHMARK T1 (U) FOR NORTHING(N), EASTING(E), HEIGHT(H), RMS FOR THE HORIZONTAL PLANE(2D) AND RA. | 22 |
| FIGURE 13 - M1B STANDARD DEVIATION OF OBSERVATIONS..... | 22 |
| FIGURE 14 - M1B DEVIATIONS FROM THE BENCHMARK T1..... | 23 |
| TABLE 7 - M1B RATIO BETWEEN T1 AND DISTANCE TO THE RECEIVER ALONG THE HORIZONTAL PLANE..... | 23 |
| TABLE 8 - M2A MEAN COORDINATES, RA AND STANDARD DEVIATION (U) FOR NORTHING(N), EASTING(E), HEIGHT(H), AND HORIZONTAL PLANE(2D)..... | 24 |
| TABLE 9 - M2A AVERAGE SIZE OF DEVIATION (D) FROM BENCHMARK T1 AND RMS FOR NORTHING(N), EASTING(E), HEIGHT(H) AND HORIZONTAL PLANE(2D)..... | 24 |
| FIGURE 15 - M2A AVERAGED COORDINATES PLACEMENTS IN RELATION TO THE BENCHMARK T1. | 25 |
| FIGURE 16 - M2A SCATTER PLOT OF OBSERVATIONS PRESENTED AS DEVIANCES FROM THE BENCHMARK T1..... | 26 |
| TABLE 10 - M2B MEAN COORDINATES, RA AND STANDARD DEVIATION (U) FOR NORTHING(N), EASTING(E), HEIGHT(H), AND HORIZONTAL PLANE(2D)..... | 27 |

| | |
|---|----|
| TABLE 11 - M2B AVERAGE SIZE OF DEVIATION (D) FROM BENCHMARK T1 AND RMS FOR NORTHING(N), EASTING(E), HEIGHT(H) AND HORIZONTAL PLANE(2D). | 27 |
| FIGURE 17 - M2B AVERAGED COORDINATES DEVIATION FROM BENCHMARK T1. | 28 |
| FIGURE 18 - M2B DEVIATION FROM THE BENCHMARK T1. | 29 |
| TABLE 12 - M3A THE BENCHMARKS AND STANDARD DEVIATIONS (U) FOR CORNERS 1, 2 AND 3. | 30 |
| TABLE 13 - M3A MEAN COORDINATES AND STANDARD DEVIATION (U) FOR NORTHING(N), EASTING(E), HEIGHT(H), AND HORIZONTAL PLANE(2D). | 30 |
| TABLE 14 - M3A AVERAGE SIZE OF DEVIATION (D) FROM BENCHMARK T1 AND RMS FOR NORTHING(N), EASTING(E), HEIGHT(H) AND HORIZONTAL PLANE(2D). | 31 |
| FIGURE 19 – M3A THE DEVIATIONS FOR ALL CORNERS AND OBSERVATIONS FROM THEIR RESPECTIVE BENCHMARKS. | 31 |
| TABLE 15 - M3B MEAN COORDINATES AND STANDARD DEVIATION (U) FOR NORTHING(N), EASTING(E), HEIGHT(H), AND HORIZONTAL PLANE(2D). | 32 |
| TABLE 16 - M3B AVERAGE SIZE OF DEVIATION (D) FROM BENCHMARK T1 AND RMS FOR NORTHING(N), EASTING(E), HEIGHT(H) AND HORIZONTAL PLANE(2D). | 32 |
| FIGURE 20 - M3B THE DEVIATION FOR ALL THE CORNERS AND OBSERVATIONS FROM THEIR RESPECTIVE BENCHMARKS. | 33 |
| TABLE 17 - M4 MINIMUM AND MAXIMUM VALUES FOR COORDINATES AND HEIGHTS WITH THE DIFFERENCE. | 34 |
| TABLE 18 - M4 STANDARD DEVIATIONS FOR EACH OBSERVATION SERIES. | 34 |
| TABLE 19 - M4 STANDARD DEVIATION FOR ALL THE OBSERVATIONS. | 35 |
| FIGURE 21 - M4 MANHOLE OBSERVATIONS SERIES COMPARED TO AN AVERAGED POINT FROM THE OBSERVATIONS. | 35 |

Abbreviations & terms

| | |
|----------|---|
| Attitude | Orientation |
| CPOS | Kartverkets network-RTK |
| DOP | Dilution of Precision |
| ETPOS | Stored GNSS-data from base-stations in Norway |
| GNSS | Global Navigation Satellite Systems |
| IMU | Internal Motion Unit |
| INS | Inertial Navigation System |
| MEMS | Micro Electrical Mechanical Sensor |
| RA | Receiver Angle, producers stated accuracy of the sensor |
| Rover | Typical Kinematic Mode |
| RTK | Real Time Kinematic |
| VRS | Virtual Reference Station |

1 Introduction

1.1 Background

In recent years there has been a surge in the use of tilt-compensated GNSS-receivers (Carlson, 2021; CHCNAV, 2021; Comnav, 2021; Hi-Target, 2021, p. ; Horizon, 2021; Leica, 2021; SatLab, 2021; Tersus GNSS, 2021; Topcon, 2021; Trimble, 2021). While GNSS-receivers make it possible to accurately determine coordinates efficiently, historically the GNSS-receivers need to be perfectly levelled above a point to measure it accurately. In addition to using less time levelling, the ability to tilt and measure points which otherwise would not be possible to measure with GNSS receivers is a highly attractive option. As most points which are “hidden” can only be measured using other solutions which are substantially more time consuming. Points that are not possible to measure with conventional GNSS such as corners of buildings, manholes and other points where the rod with the receiver is not levelled are defined as “hidden”. The points can be measured using other methods, such as defining several GNSS benchmarks nearby and then using a total station to define the “hidden” points.

The receivers have different solutions which in turn give varying levels of possible tilt and accuracy. As this is a relatively new technology there is little research available about its use. We believe this thesis can suggest how well this technology works in some situations. To gain a stronger understanding we have decided to use two types of receivers. To avoid bias they will be noted as “A” and “B”. Receiver A uses an IMU and a digital compass which allows it to accurately compensate for up to 15° on the rod. Receiver B has an inertial navigation system and a stated accuracy up to 30°, but can be tilted further with an unknown reduction in accuracy.

1.2 Purpose

Given the desirability of tilt compensated GNSS, this study explores possible use and positional uncertainty. This thesis will look at positional uncertainty by testing the equipment through four different methods. M1 investigates the effects of varying the tilt of the receiver on the rod. M2 examines the effect of tilting the receiver towards different cardinal directions. M3 measures building corners and is an actual test of a “hidden point” that would not be possible to measure with a classical GNSS-receiver. M4 measures a point in a manhole, where a conventional GNSS-observation also would not be possible. To show the effect of the device on accuracy, M1 and M2 were done in a situation with optimal satellite visibility to avoid that

as a source of error. For M3 and M4 the observations were done in an environment with more limited satellite visibility. The points in M3 and M4 being observed were hidden points. This was supposed to mimic a more challenging field environment.

Points of interest:

1. Achieved positional uncertainty with varied tilt.
2. Effect of tilt towards cardinal directions with regards to positional uncertainty.
3. Reliability of tilt compensation when used in a challenging observation environment.

1.3 Limitations

Currently there are many different technologies for tilt-compensated GNSS-receivers, this study is limited to two separate receivers. The models will not be named for either instrument and it is also important to note that this is not a comparison of the two. The receivers have different recommendations for maximum angles and different solutions for how to compensate for tilt. Statistical significance requires a larger number of observations.

1.4 United Nations - Sustainable Development Goals

Goal number 9: *Build resilient infrastructure, promote inclusive and sustainable industrialization and foster innovation*, is relevant for our thesis (United Nations, 2021). The world is experiencing global warming and infrastructure needs to be updated accordingly (Zimmerman and Faris, 2010; Amin and Watkins, 2018). Tilt-compensated GNSS sensors can increase efficiency in terms of time. More efficient, accurate surveyors cut costs and increase productivity so more money can be allocated to higher quality infrastructure.

2 Theory

2.1 Static measurements

Classic static observations as defined by Kartverket, require a minimum of 2 receivers logging simultaneously in their respective points. The observations contain phase-measurements comprised of the L1 and L2 band wavelengths (Skogseth and Norberg, 2014). The observations are recorded internally in each receiver, logged at 1 second intervals. After the measurements are complete, the data is processed by specialized software that creates vectors between the points. Using a dual-frequency receiver and a measuring period of 24 hours, it is possible to achieve an accuracy of 2-4 mm in the horizontal plane. With a significant reduction of measuring time the horizontal accuracy can be kept, although the height is effected more (Kartverket, 2009).

ETPOS is a subscription service of Kartverket which contains the preceding three months' worth of GNSS-observations from the permanent reference stations (Kartverket, 2020b). The data is logged at 1-, or 30-second intervals.

2.2 Network RTK

The network RTK method is commonly used to achieve high accuracy within short periods of time using GNSS. Accuracy from the CPOS network RTK is typically given at cm-level (Kartverket, 2020a). The network consists of permanent GNSS receivers that continuously stream satellite observations to a central server in which combined data is used to generate RTK corrections for precise positioning use within the area of coverage (Berber and Arslan, 2013). Combined data includes the corrections of the carrier phase ambiguities, primarily due to the atmospheric conditions and satellite orbits. Using differential techniques where a station with known coordinates is used as a reference is effective in reducing errors (Lachapelle and Alves, 2002). Correctional data is calculated from the VRS and transferred via the NTRIP-protocol. Using the baseline position of the rover on connecting with CPOS, the closest reference stations are found. With both rover and server internet-connected, the rover sends its position to the server, it is possible to calculate a VRS close to the rover. The VRS is ideally as close as possible to the rover. The distance limit for CPOS is 5 km (Kartverket, 2021).

CPOS is a network of GNSS reference stations spread across Norway. The accuracy this service offers is as follows: 8 mm horizontally (66% confidence) and 17-20 mm vertically (66% confidence) when the network reference stations are within 35 km (Kartverket, 2020a).

Common areas of use include sewage and water by both municipalities and commercial companies. The commercial companies often have an accuracy requirement of ± 3 cm along the horizontal plane and ± 5 cm in height (Powel, 2018). Municipalities sometimes have a lower requirement at 10 cm on the horizontal plane and height accuracy of ± 5 cm for Indre Østfold Kommune (2021). Another area is the use of property measurements, Kartverket (2011) gives the requirement of 10 cm along the horizontal plane as an accuracy requirement.

2.3 Hardware

2.3.1 Receiver A

As mentioned in the introduction, receiver A has a maximum tilt angle of 15° . Within these angles the accuracy decreases by 5 mm plus 1.3 mm per degree tilt in angles that are 10° or less. With angles that are greater than 10° tilt the accuracy is decreased by 1.8 mm per degree. This means that for an angle of 5° the accuracy is decreased by 11.5 mm, for 10° the value becomes 18 mm and for 15° the value becomes 27 mm.

Table 1 - Producers horizontal stated accuracy for levelled RTK (L1+L2) and Compensator Tilt Sensor uncertainty.

| HORIZONTAL | HORIZONTAL TILT < 10° | HORIZONTAL TILT $\geq 10^\circ$ |
|-------------------|---|---|
| 5 MM + 0.4 PPM | 1.3 mm/ $^\circ$ Tilt | 1.8 mm/ $^\circ$ Tilt |

Receiver A uses an electronic compass and a calibration process that is required each time the equipment is used. This is a magnetometer-based technology where the rod's angle and direction are decided by magnetic north. With an electronic compass and a tilt calibration, movement is not required to use the tilt-function although magnetic disturbances pose a limitation. Positional inaccuracy when using RTK is 5 mm + 0.5 ppm for horizontal and 10 mm + 0.8 ppm for vertical.

2.3.2 Receiver B

Receiver B decides the rod's direction by measuring acceleration and rotation of the accelerometers and gyroscopes. These combined are the IMU. The receiver requires movement to function but requires no calibration and is not affected by magnetic disturbance. Tilt is determined using vector-based algorithms which calculate the position at the tip of the rod. The

input for the algorithm includes the rod's length, measured position of the phase-centre of the GNSS-antenna and antenna attitude.

Receiver B has a stated accuracy of 8 mm with an additional 0.4 mm inaccuracy per degree of tilt up to 30°. The initial inaccuracy is rather large, worth noting how the accuracy decrease rises at a relatively slow rate. Positional inaccuracy when using network RTK is at 8 mm + 0.5 ppm for horizontal and 15 mm + 0.5 ppm for vertical.

Table 2 - Producers horizontal stated accuracy for levelled RTK(L1/L2), and Compensator Tilt Sensor uncertainty.

| HORIZONTAL | HORIZONTAL TILT < 30° |
|-------------------|---------------------------------|
| 8 MM + 0.5 PPM | 0.4mm/° |

2.3.4 IMU and INS

IMU are usually a combination of a gyroscope, accelerometer and sometimes a magnetometer or GNSS-equipment (SBG Systems, 2020). An IMU measures the inertial gravitational forces in a device to calculate its movement and keep track of its position and orientation in space. An INS has the same function as an IMU, but does not rely on external signals like GNSS. The absolute attitude is only calculated with the internal sensors relative to a known starting point (Kjerstad, 2021).

Receiver A has a 9-axis IMU with gyroscope, accelerometer, and a 3-axis compass. The second rover only uses a gyroscope and an accelerometer. To compensate for the lack of a compass, it relies more on the INS which uses an algorithm with input from the gyroscope, the accelerometer and GNSS logging to continuously keep track of the rovers attitude while the tilt compensation is turned on (Luo *et al.*, 2018). The INS calculates a relative attitude from a known absolute attitude. The known position is given from RTK-logging and the known orientation is measured by the gyroscope and accelerometer.

This means that, to work properly, the tilt compensation depends on a stable RTK connection during the observations. The inertial navigation system in the receiver does not work well enough by itself to securely decide the absolute attitude of the receiver if the known position is not updated frequently with RTK.

2.4 Sources of error

The accuracy of GNSS is directly correlated to a geometrical parameter known as DOP. DOP is decided by the distribution of satellites visible above the receiver. Four or more visible satellites are required for solving the clock offset and three dimensions of the receiver's position. If the four (or more) satellites are crowded together the DOP-value would be high, indicating high uncertainty of the position. In a perfect world a satellite is directly above the receiver, and the others are 120° from each other in azimuth near the horizon (Van Sickle, 2021b).

Atmospheric conditions are one of the largest sources of error, the main contributing factors being the ionosphere and troposphere (Van Sickle, 2021a). Both sources disturb the signal in their respective ways. Errors stemming from the atmosphere are avoided by mission planning and mask angles. Mask angles are generally recommended to be 15-20°, as to avoid satellites near the horizon as their signals travel the furthest through the atmosphere.

To calculate a precise position with GNSS, the signals need to travel directly from the satellite to the receiver. Objects in the vicinity of the receiver may reflect some signals before they enter the antenna, causing disturbances in pseudorange and carrier phase observations. Although modern receivers have several methods for recognising and ruling out reflected signals, some signals may go undetected and cause errors. Rooftops, for example, are known to be bad multipath environments due to vents and other reflective objects within the antenna's field of view (Leick, Rapoport and Tatarnikov, 2015).

2.5 Aspects of Data-processing

The main analysis is based on calculation of the mean, standard deviation, RMS and mean deviation processed in Excel. Kartverket's suggestion for presenting accuracy is showing the systematic deviances, standard deviations and gross errors (Kartverket, 2015).

The mean can also be referred to as average and is calculated with the following equation.

$$\bar{x} = \frac{1}{n} \sum_{i=1}^n x_i$$

Standard deviation indicates the spread (variation) of a group of observations or calculated values in relation to their true or estimated value. The following formulae is for the relation of

the estimated value. Number of observations in the dataset n , the observation in the dataset i , and \bar{x} is the mean of the observations (Kartverket, 2015).

$$u = \sqrt{\frac{\sum(x_i - \bar{x})^2}{n-1}}$$

The *RMS* is a measurement of how the values scatter from the “true” value. With this method we can see how much the coordinates of the observations deviate from the “true” coordinates. If the values that are squared are true deviances, RMS will give the same value as the standard deviation. When systematic deviations are removed, the RMS will give a lower value than the standard deviation. RMS functions as an unbiased estimator exclusively when we have “true” deviations, otherwise it shows a better quality than what is actually the case (Kartverket, 2015). In the formulae below ε is the value of an observation minus the control value (reference point).

$$RMS = \sqrt{\frac{\sum \varepsilon^2}{n}}$$

RMS or standard deviation is calculated for both Northing, Easting and Height. The mean deviation, standard deviation and RMS has a combined calculated value for the horizontal plane (2D) with the following formula (Ohlsson, 2014).

$$2D = \sqrt{a_N^2 + a_E^2} \quad \text{Where } a = RMS, u_x \text{ or } \bar{x}.$$

Mean values, standard deviation, RMS and mean deviation for each coordinate relative to the reference coordinates were calculated. A gross error test was performed in GISLINE where some observations were marked to be removed. The gross error test uses a multiple t-test which functions where each observation has a calculated gross error and a mean error of the gross error. The size of the values are then used statistically to decide if the observation has a gross error (Norkart, 2021).

The deviation from the tip of the rod to receivers’ position is calculated through the following process. Assuming the rod is 2 metres long, and t is the degree of tilt, the formula becomes.

$$\Delta b = \sin(t) * 2$$

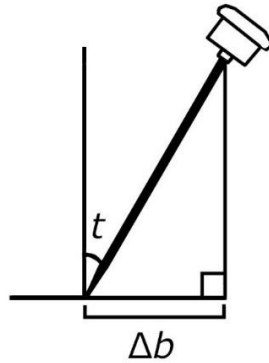


Figure 1 - Variables for estimating distance from antenna receiver to reference point in the ground plane. (Figure: Sveinung Karlsen, 2021).

With this “true” value (Δb) it is possible to look at the ratio between the true distance from the tip of the rod to the receiver and the observations along the horizontal plane (Δa). The observations are averaged to see the deviation from the reference point. A comparison of actual tilt-compensation required and the amount the device corrects for. The relation between Δa and Δb are compared by dividing the “true” value by the measured value to calculate the ratio of the values for each degree of tilt.

2.6 Previous studies

High-precision RTK Positioning with Calibration-Free Tilt Compensation (Luo et al., 2018)

Tilt-compensated GNSS-receivers are relatively new and there is a limited amount of scientific research regarding this technology. Here the drawbacks of magnetometer-based approach are mentioned. This approach has problems seeing as magnetic North is not the same as geographical North. Additionally, the magnetometer is highly susceptible to magnetic disturbances created by ferrous metals and electrical currents. This essentially means the receiver needs to be calibrated frequently. Luo et al. argue for using an INS to determine the attitude of the rod in real time, to collect data from the MEMS IMU.

The receiver was tested in environments with an open-sky or severe multipath and compared to a conventional GNSS receiver. In the clear view test the positional uncertainty was at 24 mm for tilted observations compared to 21 mm for levelled receivers. The severe multipath environment was done with over 200 observations near a building with a metal facade. In this experiment the tilted-receiver had 15% more RTK-fixed solutions and on average a 50% better

positioning accuracy. It is important to note that the results were due to; high-sensitivity GNSS signal tracking, larger distance of antenna to the building resulting in lower multipath frequency for points closer than 10 cm to the building.

Lägesosäkerhet vid nätverks-RTK-mätning med inbyggd lutningskompensator: en undersökning av Leica GS18 T (Almstedt and Peterson, 2019)

Almsted and Peterson explored several of the same tests as the present study. They explored observations with varying degrees of tilt and found a positional accuracy of 35 mm at 20° and 66 mm or 71 mm at 30° on the horizontal plane. For testing the cardinal directions, it was found that the deviation in easting has a greater effect on the mean deviation from the reference point in the plane rather than northing when tilted to the south. Tilt towards the east gave larger deviations in northing rather than easting. Almstedt and Peterson (2019) found in the cardinal directions that the deviation is the greatest for the coordinate that is perpendicular to the direction of the tilt, except for tilt to the west, though they could not conclude as to what the reason is.

They conclude that the direction in which the instrument is tilted effects the positional uncertainty: with the mean deviation on the horizontal plane being the lowest when the instrument is tilted to the north and west and highest when tilted to the south and east, 2-3 mm and 9 mm respectively. They also suggest testing the cardinal directions and its effect to a greater extent, as well as measuring building corners of taller buildings to examine multipath or low visibility effects.

Testing the accuracy and usability of the GNSS receiver Leica GS18 I (Myslivec, 2021)

Myslivec examined the accuracy and the reliability of the tilt compensation and the photogrammetry function. This master's thesis consisted of two methods of checking the accuracy of the GNSS receiver, one where it compared both "regular" levelled observations and levelled observations with the tilt compensation on with tilted observations at 45° and 90°. The other method was to hold the receiver completely still and see if there was any degradation of the observations, this was done at a 45° angle and with the rod in completely horizontal and vertical positions.

Myslivic found that even when doing observations, the traditional way with the rod levelled and the tilt compensation activated would result in a better accuracy. Myslivec also concludes

that a 45° tilt achieves an accuracy usable for many surveying purposes, and in smaller degrees of tilt there is almost no restriction on use (Myslivec, 2021).

Observability of error States in GPS/INS Integration (Hong et al., 2005)

Hong et al. (2005) examined uncertainties in attitude, gyro bias, and GPS antenna lever arm to determine unobservable errors in the position, velocity, and accelerometer bias. Demonstrating errors are made observable by manoeuvring. Acceleration changes improved the estimate of attitude and gyro bias and changes in angular velocity enhanced the lever arm estimate. It is also noted how using an accelerometer for measuring the orientation of the rod with respect to geographic north is a challenging task.

3 Method

3.1 Reference points

Reference points with 3 hours static measurements and the ETPOS bases as base stations for the vector calculations were established. The ETPOS base stations used, consisted of:

BROT – Brøttum DOKK – Dokka HAMR – Hamar MOEC – Moelv SKRC - Skreia

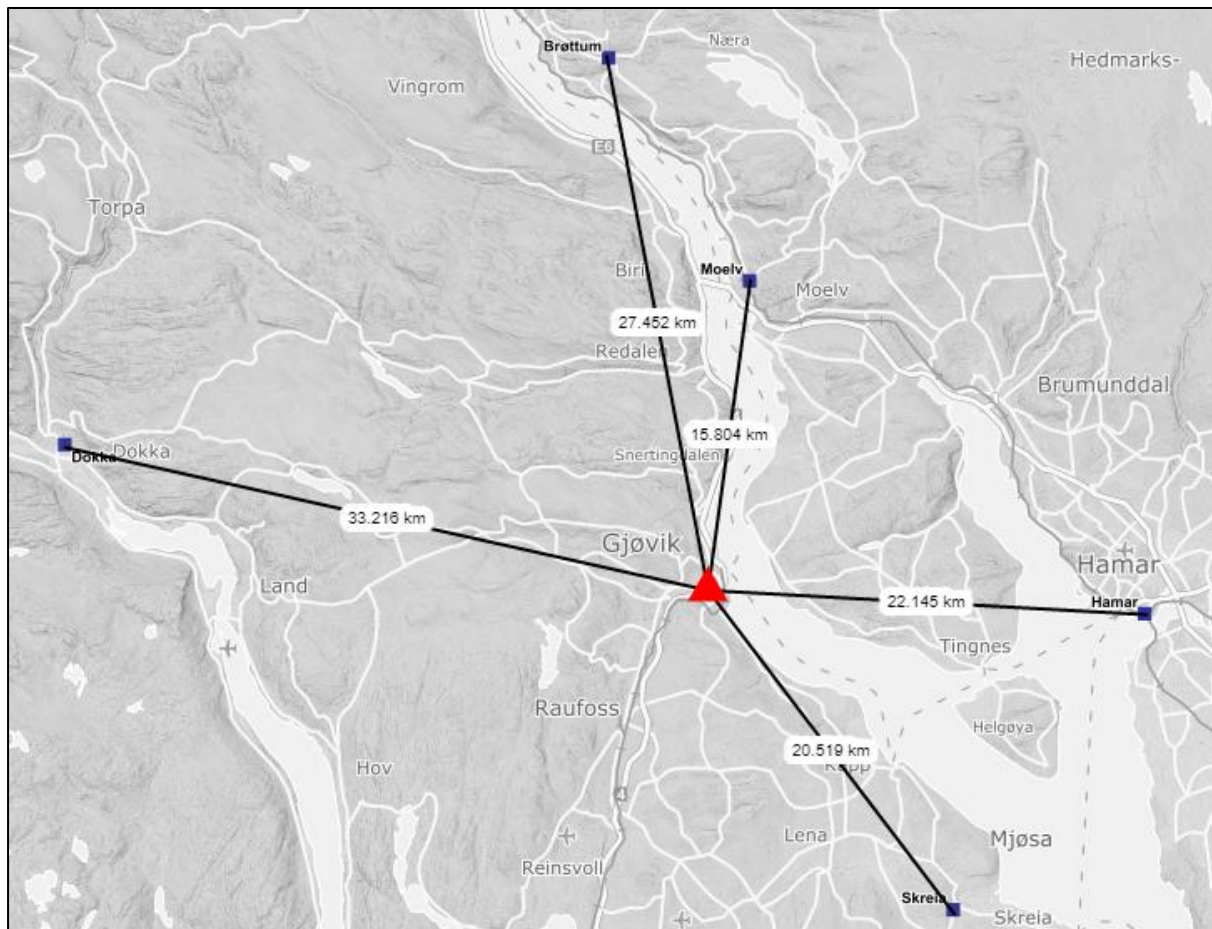


Figure 2 - Map snippet collected from Norgeskart.no visualizing base stations distance in addition to where most of the observations took place (red triangle).

Five points were established, *TI*, *PI*, *GI*, *S2* and *S3* using static observations. The observations were done over several days, on the 9th, 10th and 12th of February in addition to the 16th and 17th of March 2021. To avoid potential bias towards either receiver, a third receiver of a different model was used for the observations. All observations were then imported into Leica Infinity where the vectors were created, analysed, and eventually equalized.

The reference points were used for two purposes, one point (*TI*) was established in a position on a roof that had an unobstructed view of the sky in all cardinal directions and was used for

measurements during method 1 and method 2. Four others (*PI*, *GI*, *S2* and *S3*) were established in the campus area and were intended for establishing coordinates for the building corners.

T1 was a thumbtack placed on the G-building roof. *PI* and *GI* were created with asphalt nails hammered into the pavement. *S2* and *S3* were on previously existing pillars. All the points are located within the NTNU Gjøvik campus area.



Figure 3 - *T1* and *P1* (Photo: Jakob B Kristiansen, 2021)

The ETPOS base stations and static measurement for the reference points were used for which we had an expected quality of sub-cm accuracy. In comparison to CPOS measurement with an expected quality of around 1 cm in the horizontal plane and 2 cm in height (Kartverket, 2020a).

Establishing coordinates to be used as benchmarks for the building corners were done with a MS60 total station. Free stations were done at three different points to be able to define the coordinates for the building corners.



Figure 4 -The G building. *T1* was established on the balcony on the lower roof. (Photo: Jakob B Kristiansen, 2021)

3.2 Method 1 – Tilt-compensation at varying degrees

For testing the tilt-compensation, measurements were performed on the same point with the same attitude and varying tilt. Through this it is possible to examine what changes happen when it is solely a difference in tilt.

The observations occurred over the span of two days where both receivers were used so they were correlated in time. Measurement sessions were made with at least 45 minutes separation to avoid correlations between the sessions (Kartverket, 2009; Odolinski, 2012). The dataset consisted of 10 sessions, where each measurement was a 3 second (3 epochs) measurement.

The two receivers were tilted at different degrees during the sessions, receiver A at 0° , 5° , 10° and 15° , receiver B at 0° , 10° , 20° , 30° and 40° . All the observations were tilted in the same cardinal direction south-west, due to it having the least amount of obstructions to the sky. The observations were done on the reference point *T1* with the receivers on 2-metre rods. The tilt-compensator was active during all the measurements for both receivers, including the 0° observations.

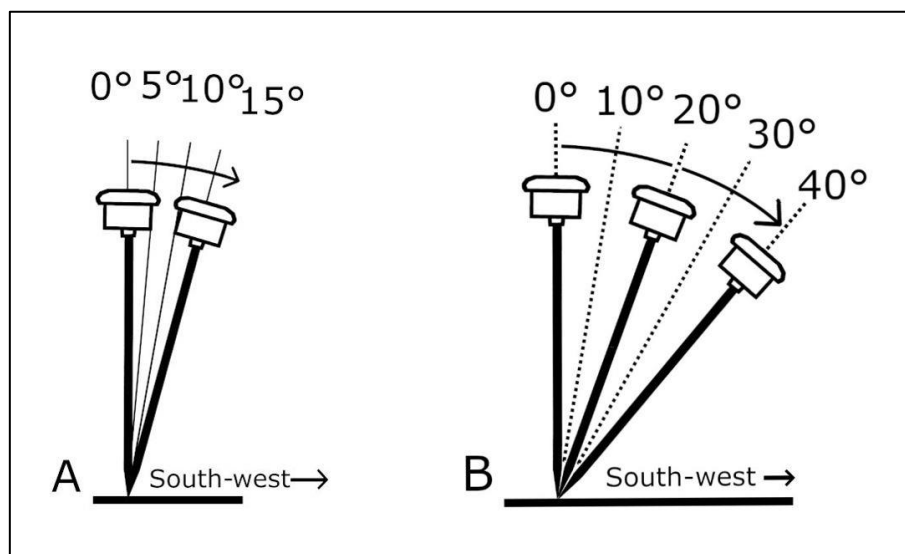


Figure 5 - Model of M1 in practice. (Figure: Sveinung Karlsen, 2021).

3.3 Method 2 – Visible satellite bias for cardinal directions

This method was chosen due to GNSS constellations not having equal amounts of satellites in all parts of the sky. With this method it is possible to see if there is a significant difference in achieved accuracy and precision with regards to cardinal direction.

Measured on the same days as method 1, and in the same sessions as in method 1. Both receivers were tilted to their “max”, which for receiver A was 15° and receiver B was 30° and then oriented in the different cardinal directions, North South East and West. Similarly, method 1 was performed on the *T1* reference point which had an unobstructed view of the sky.

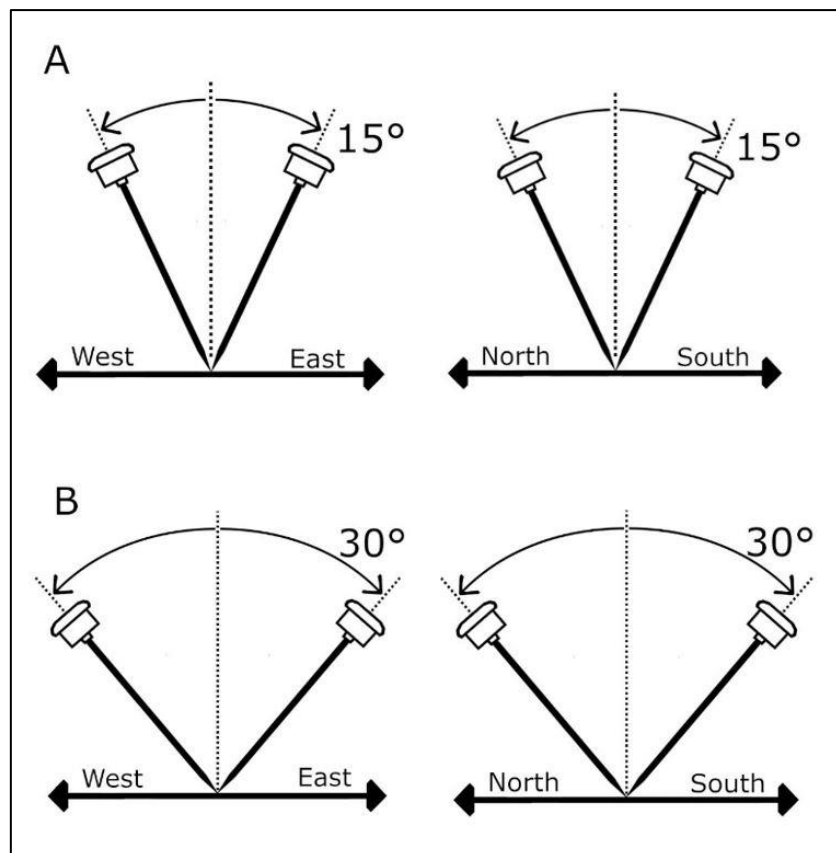


Figure 6 - Model of M2 in practice. (Figure: Sveinung Karlsen, 2021).

3.4 Method 3 – Measuring building corners

Three separate corners were measured around the main university building. The decision was influenced by the suggestion of measuring a building with a height of over 9m (Almstedt and Peterson, 2019). The building corners that were chosen to measure was the S-building and H-building at the NTNU Gjøvik Campus. The S-building is roughly 20 metres in height and the H-building is roughly 11 metres. A part of the goal for this method was to see the performance of the tilt-compensation in different situations. Both “bad” and “good” measuring environments were required.

Corner 1 (C1) was measured between two large buildings (S-building and H-building). The aim was to replicate a measurement in a city environment. The receiver was tilted towards the Southern direction which is toward the lowest building (H). The measuring point was on the S-building.

Corner 2 (C2) is also placed on the S-building, the corner on this side of the S-building is more open. The rod was tilted in a South-West direction which has a clearer horizon than corner 1, but there are still some obstructions.

Corner 3 (C3) is on the West side of the S-building and is tilted towards an unobstructed sky in the North-West direction. In comparison to the other corners this would be more of a situation where a tall building is measured in an otherwise “good” measurement environment.



Figure 8 - The H and S buildings (Photo: Jakob B Kristiansen, 2021)

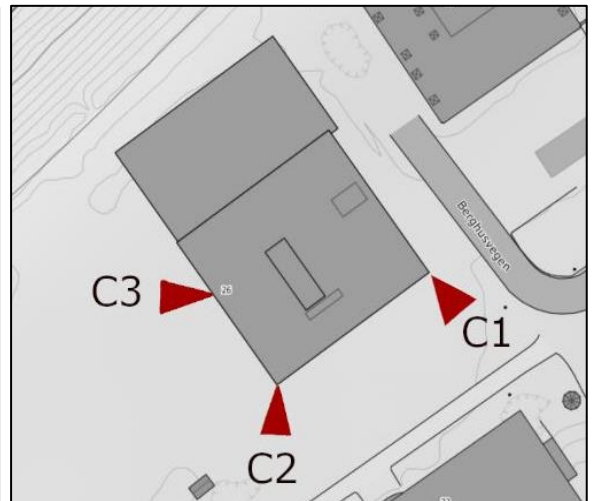


Figure 7 - Building corners with approximate direction of tilt indicated by the arrows.

3.5 Method 4 - Manhole

This method was chosen as an experiment for a real-life situation. Measuring points in manholes can be cumbersome as they are sometimes challenging to measure directly with GNSS receivers. The point in the manhole has a relatively poor observation environment, this can decrease the expected accuracy and precision. Worth noting how we did not establish a benchmark, in addition to not being able to properly mark the measurement spot. Some deviation will come from not measuring the exact same point due to sight issues in different light conditions.

This method consisted of 15 sessions at 15° for 3 second measurements and consisted of 10 or more measurements in each session. To access the pipe in the manhole it was necessary to use a long rod, in this case a 4.65-metre-long rod.

Receiver A was not used for this method as we did not have access to it at this point.

Since every session consisted of 10 or more observations, a gross search was performed in GISLINE. The measurements in a session are correlated and should not contain any gross errors. Any gross errors would indicate issues with the entire session unless it could be explained by user error.



Figure 9 - Manhole, the point that was measured was on top of the pipe. (Photo: Sveinung Karlsen, 2021)

4 Results

All values are given in metres and coordinates in EUREF89 UTM32 NN2000 unless stated otherwise.

Standard deviation is a measure of the spread or precision of the observations while RMS and the average deviation from the benchmark both describe the accuracy of the observations.

4.1 Reference points

Tl was measured over a period of three sessions to be determined more accurately. The reference points achieved an estimated standard deviation of 6 millimetres or less in the horizontal plane.

Table 3 - Reference points coordinate after the adjustment calculation in addition to standard deviation (*U*).

| | N [m] | E [m] | H [m] | U(N) [m] | U(E) [m] | U(H) [m] |
|-----------|------------------------|------------------------|------------------------|---------------------------|---------------------------|---------------------------|
| T1 | 6 740 523.071 | 591 576.955 | 195.784 | 0.002 | 0.001 | 0.004 |
| P1 | 6 740 485.067 | 591 514.179 | 182.948 | 0.005 | 0.004 | 0.011 |
| G1 | 6 740 392.903 | 591 440.192 | 183.368 | 0.002 | 0.001 | 0.004 |
| S2 | 6 740 432.895 | 591 387.516 | 183.481 | 0.004 | 0.003 | 0.008 |
| S3 | 6 740 518.278 | 591 466.552 | 184.149 | 0.003 | 0.003 | 0.006 |

4.2 Method 1 – Tilt-compensation of varying degrees

4.2.1 Receiver A

The dataset had a single gross error removed from the observations with 10° tilt.

Table 4 and Figure 10 show the standard deviation,

Table 4 also shows the average deviation from the benchmark as well as the RMS of the horizontal plane. The standard deviation shows a higher precision for observations without tilt, but the precision seems stable for all amounts of tilt. The height seems to be consistent

regardless of the degree of tilt. Of note here, is the increase for both RMS the average deviation from the benchmark when the tilt increases.

Table 4 - MIA Standard deviation and average size of deviation (D) from benchmark T1 (U) for Northing(N), Easting(E), Height(H), RMS for the horizontal plane(2D) and RA.

| | U(N) [m] | U(E) [m] | U(H) [m] | D(N) [m] | D(E) [m] | D(H) [m] | RMS(2D) [m] | RA [m] |
|-----|-------------|-------------|-------------|-------------|-------------|-------------|----------------|-----------|
| 0° | 0.007 | 0.010 | 0.024 | -0.004 | 0.009 | -0.023 | 0.015 | 0.005 |
| 5° | 0.028 | 0.012 | 0.026 | -0.023 | 0.068 | -0.023 | 0.077 | 0.012 |
| 10° | 0.027 | 0.015 | 0.024 | -0.049 | 0.154 | -0.023 | 0.164 | 0.018 |
| 15° | 0.028 | 0.009 | 0.016 | -0.053 | 0.222 | -0.018 | 0.230 | 0.027 |

Figure 10 visualizes the standard deviation from

Table 4, and the highest precision is for observations with a levelled rod. For measurements with tilt the observations are consistently less precise in northing than easting. The precision when using the tilt-function stays relatively stable for the observations 5°, 10° and 15° tilt.

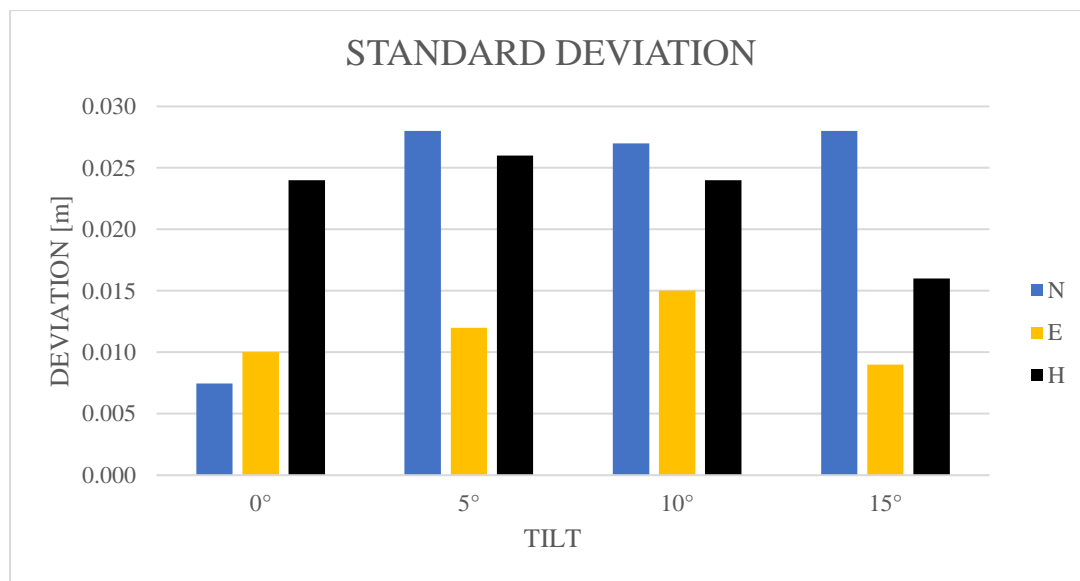


Figure 10 - MIA Standard deviation of observations.

Figure 11 visualizes how the average deviation from the benchmark for both northing and easting increase with increased tilt. The easting coordinate increases substantially more than the northing and the height is seemingly unaffected.

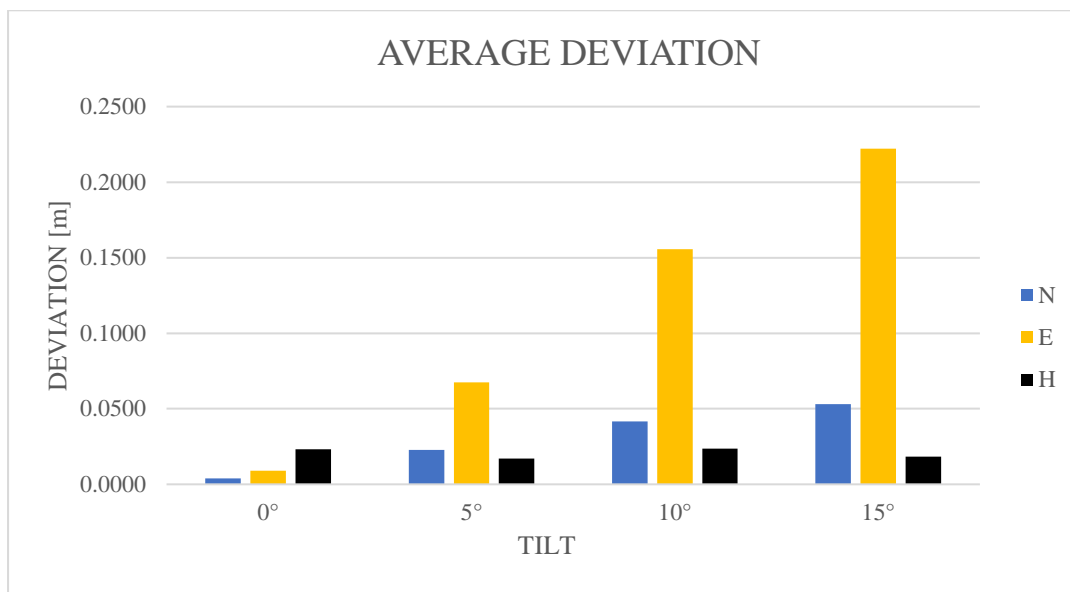


Figure 11 – MIA Average deviation from TI.

Figure 12 visualizes the deviations of the observations in relation to reference point *T1*. The observations with the same amount of tilt are quite precise relative to each other. With regards to accuracy, the plot shows a considerable deviation from the reference point of the inclined observations. The observations performed without tilt are accurate, while the other observations deviate from the reference point increasingly with greater degree of tilt.

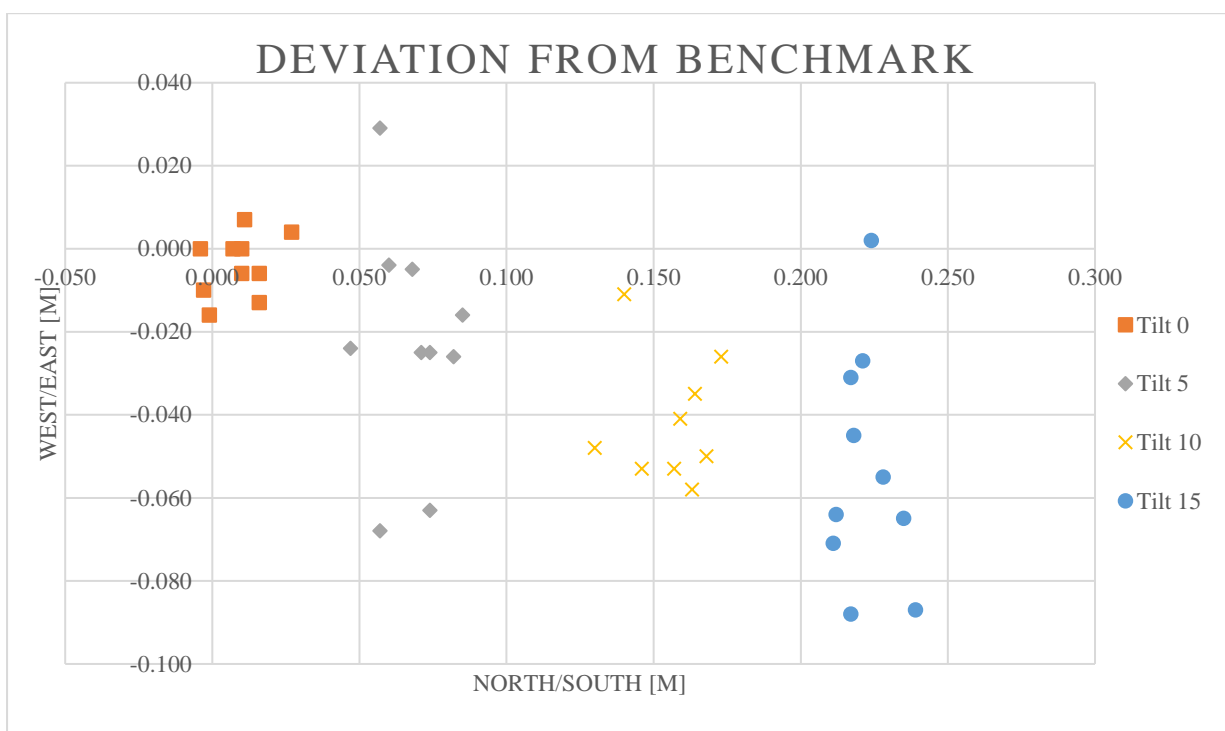


Figure 12 - MIA Scatterplot of the deviations of observations from the benchmark *T1*.

Table 5 shows how the measured coordinates on average are about half as far from the reference point in the horizontal plane as the receiver itself, regardless of tilt. Roughly 50-60% of the actual distance has been compensated by the tilt-function.

Table 5 - Ratio between *T1* and distance to the receiver along the horizontal plane

| | ΔA [m] | ΔB [m] | RATIO [m] |
|----------|-------------------|-------------------|--------------|
| 0 | 0.010 | 0 | - |
| 5 | 0.071 | 0.174 | 0.409 |

| | | | |
|-----------|-------|-------|-------|
| 10 | 0.161 | 0.347 | 0.464 |
| 15 | 0.228 | 0.518 | 0.441 |

4.2.2 Receiver B

All observations with tilt were removed from set eight and nine due to gross error, as well as two observations from set five. Table 6 shows how there is a relatively low standard deviation within the observations themselves, and how the easting values are the most uncertain. The deviation of the observations compared to the benchmark increases with each degree of tilt beyond 10° observations.

Table 6 - M1B Standard deviation and average size of deviation (D) from benchmark T1 (U) for Northing(N), Easting(E), Height(H), RMS for the horizontal plane(2D) and RA.

| POINT | U(N) [m] | U(E) [m] | U(H) [m] | D(N) [m] | D(E) [m] | D(H) [m] | RMS(2D) [m] | RA [m] |
|-------|-------------|-------------|-------------|-------------|-------------|-------------|----------------|-----------|
| 0° | 0.009 | 0.005 | 0.009 | -0.012 | -0.013 | -0.010 | 0.020 | 0.008 |
| 10° | 0.006 | 0.006 | 0.013 | -0.013 | -0.013 | -0.012 | 0.018 | 0.012 |
| 20° | 0.009 | 0.017 | 0.011 | -0.014 | -0.013 | -0.006 | 0.026 | 0.016 |
| 30° | 0.003 | 0.018 | 0.009 | -0.014 | -0.019 | -0.010 | 0.030 | 0.020 |
| 40° | 0.005 | 0.022 | 0.012 | -0.014 | -0.020 | -0.009 | 0.032 | 0.024 |

Figure 13 visualizes how the easting value varies significantly more than the northing. Interesting how the height stays relatively stable throughout the observations. The northing variation is reduced when rod tilt increases.

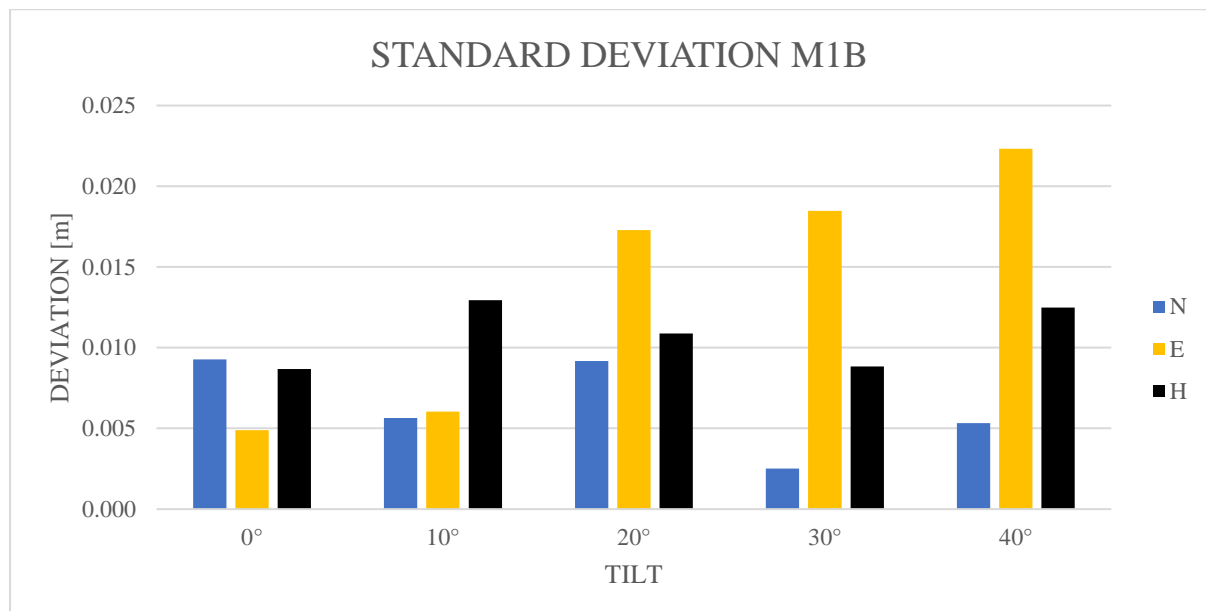


Figure 13 - M1B Standard deviation of observations.

Figure 14 visualizes how the observations tend to deviate towards south-west from *T1*. There are some outliers within the more inclined observations. The 40° observations have the highest amount and largest deviations.

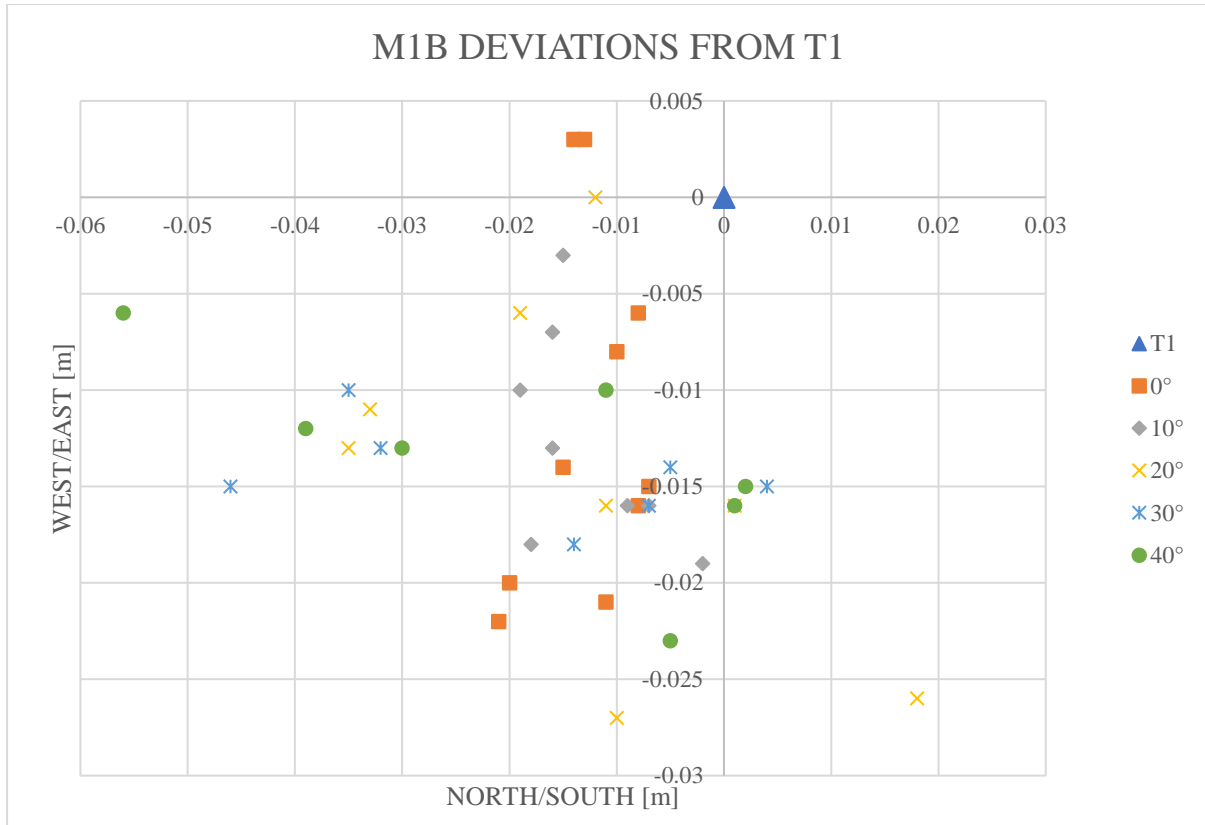


Figure 14 - M1B Deviations from the benchmark *T1*.

Table 7 shows the ratio between the actual distance along the horizontal plane to the receiver. This visualizes how the tilt-compensator functions for placing the receiver over its intended point. The tilt-compensation functions for values of 94% of the change.

Table 7 - M1B Ratio between *T1* and distance to the receiver along the horizontal plane.

| | ΔA [m] | ΔB [m] | RATIO [m] |
|-----------|-------------------|-------------------|--------------|
| 0 | 0.017 | 0 | - |
| 10 | 0.020 | 0.347 | 0.058 |
| 20 | 0.019 | 0.684 | 0.028 |
| 30 | 0.024 | 1 | 0.024 |
| 40 | 0.024 | 1.286 | 0.019 |

4.3 Method 2 – Cardinal directions

4.3.1 Receiver A

For the observations tilted towards the different cardinal directions (Table 8), no observations were removed. The largest standard deviation within the dataset comes from the Easting coordinates when tilted in precisely that angle.

Table 8 - M2A Mean coordinates, RA and standard deviation (U) for Northing(N), Easting(E), Height(H), and horizontal plane(2D).

| POINT | N [m] | E [m] | H [m] | U(N) [m] | U(E) [m] | U(H) [m] | U(2D) [m] | RA [m] |
|--------------|-----------------|-----------------|-----------------|--------------------|--------------------|--------------------|---------------------|------------------|
| T1 | 6 740 523.071 | 591 576.955 | 195.784 | 0.001 | 0.001 | 0.005 | 0.002 | ... |
| NORTH | 6 740 522.985 | 591 576.766 | 195.774 | 0.018 | 0.020 | 0.016 | 0.027 | 0.027 |
| SOUTH | 6 740 523.162 | 591 577.145 | 195.778 | 0.026 | 0.014 | 0.026 | 0.029 | 0.027 |
| EAST | 6 740 523.263 | 591 576.893 | 195.772 | 0.019 | 0.043 | 0.017 | 0.047 | 0.027 |
| WEST | 6 740 522.867 | 591 577.047 | 195.773 | 0.013 | 0.028 | 0.013 | 0.031 | 0.027 |

The average deviations of the deviations from the benchmark are relatively large. Of interest, how the largest deviations for both north and south tilted observations are the easting, contrary to northing being the largest when tilted east or west.

Table 9 - M2A Average size of deviation (D) from benchmark T1 and RMS for Northing(N), Easting(E), Height(H) and horizontal plane(2D).

| DIRECTION | D(N) [m] | D(E) [m] | D(H) [m] | D(2D) [m] | RMS(N) [m] | RMS(E) [m] | RMS(H) [m] | RMS(2D) [m] |
|------------------|--------------------|--------------------|--------------------|---------------------|----------------------|----------------------|----------------------|-----------------------|
| NORTH | -0.085 | -0.188 | -0.009 | 0.206 | 0.087 | 0.189 | 0.018 | 0.208 |
| SOUTH | 0.091 | 0.191 | -0.006 | 0.212 | 0.095 | 0.191 | 0.026 | 0.213 |
| EAST | 0.193 | -0.062 | -0.012 | 0.203 | 0.194 | 0.074 | 0.020 | 0.207 |
| WEST | -0.203 | 0.092 | -0.011 | 0.223 | 0.204 | 0.096 | 0.016 | 0.225 |

Figure 15 presents the averaged coordinates of the observations in comparison to the benchmark *T1*. This figure visualizes how the observations have rotated roughly 100 degrees anti-clockwise.

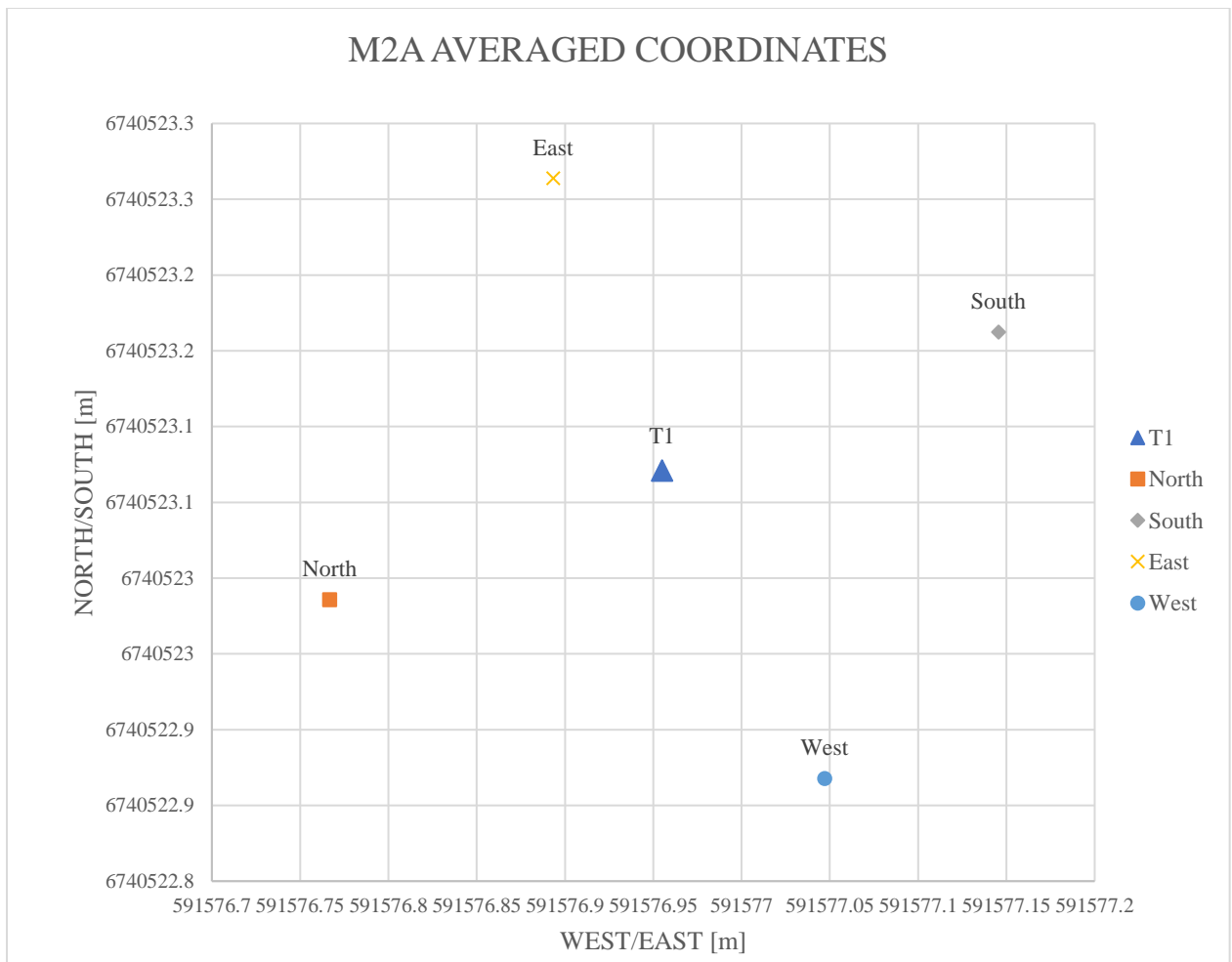


Figure 15 - M2A Averaged coordinates placements in relation to the benchmark *T1*.

Figure 16 shows how the observations are precise within their own attitude, but rather inaccurate. Also, interesting to see how the deviation from the benchmark stays roughly the same.

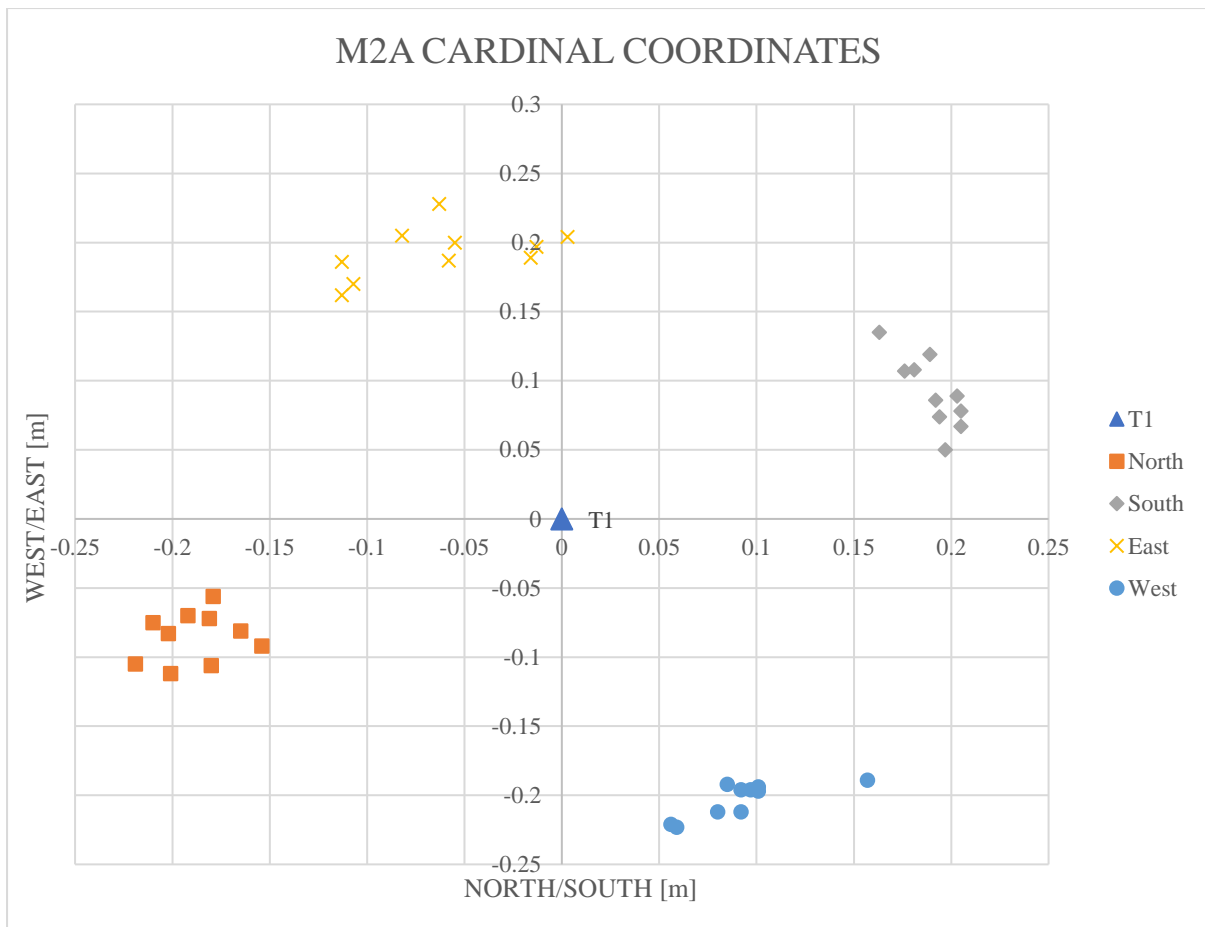


Figure 16 - M2A Scatter plot of observations presented as deviances from the benchmark T1.

4.3.2 Receiver B

Observations done during M2B had gross errors for the final two sets of observations. These were removed during the analysis. Standard deviation for each coordinate and height, as well as the horizontal plane. In Table 10, the RA value shows how much uncertainty the producer expects the receiver to have at the given angle. Interestingly, there is a smaller deviation within the observations when angled towards the west. The largest deviations being when tilted towards the north and east is the easting. While tilt towards south and west are more equal in deviation for northing and easting.

Table 10 - M2B Mean coordinates, RA and standard deviation (U) for Northing(N), Easting(E), Height(H), and horizontal plane(2D).

| POINT | N [m] | E [m] | H [m] | U(N) [m] | U(E) [m] | U(H) [m] | U(2D) [m] | RA [m] |
|--------------|------------------------|------------------------|------------------------|---------------------------|---------------------------|---------------------------|----------------------------|-------------------------|
| T1 | 6 740 523.071 | 591 576.955 | 195.784 | 0.001 | 0.001 | 0.005 | 0.002 | ... |
| NORTH | 6 740 523.055 | 591 576.929 | 195.771 | 0.009 | 0.018 | 0.008 | 0.022 | 0.020 |
| SOUTH | 6 740 523.064 | 591 576.963 | 195.776 | 0.012 | 0.012 | 0.012 | 0.017 | 0.020 |
| EAST | 6 740 523.089 | 591 576.939 | 195.773 | 0.012 | 0.031 | 0.010 | 0.033 | 0.020 |
| WEST | 6 740 523.059 | 591 576.941 | 195.769 | 0.005 | 0.004 | 0.010 | 0.006 | 0.020 |

Table 11 shows the actual size of deviations from the benchmark. Interesting to note how the easting is predominantly the furthest from the benchmark and the attitude to the south and west being the most accurate.

Table 11 - M2B Average size of deviation (D) from benchmark T1 and RMS for Northing(N), Easting(E), Height(H) and horizontal plane(2D).

| DIRECTION | D(N) [m] | D(E) [m] | D(H) [m] | D(2D) [m] | RMS(N) [m] | RMS(E) [m] | RMS(H) [m] | RMS(2D) [m] |
|------------------|---------------------------|---------------------------|---------------------------|----------------------------|-----------------------------|-----------------------------|-----------------------------|------------------------------|
| NORTH | -0.006 | -0.014 | -0.010 | 0.015 | 0.010 | 0.022 | 0.013 | 0.024 |
| SOUTH | -0.007 | 0.008 | -0.008 | 0.011 | 0.013 | 0.014 | 0.014 | 0.019 |
| EAST | -0.007 | -0.016 | -0.011 | 0.017 | 0.013 | 0.033 | 0.014 | 0.035 |
| WEST | -0.012 | -0.014 | -0.015 | 0.018 | 0.013 | 0.014 | 0.018 | 0.019 |

Figure 17 shows the averaged coordinates deviation from the benchmark *T1*. Note how the observations are predominantly drawn towards the south with the exception of the east tilted observation. The north and east tilted observations result in the largest deviations from the benchmark. The north-tilted observation is tilted along the north/south axis and receives a larger error along the west/east axis, vice versa for the east-tilted observation.

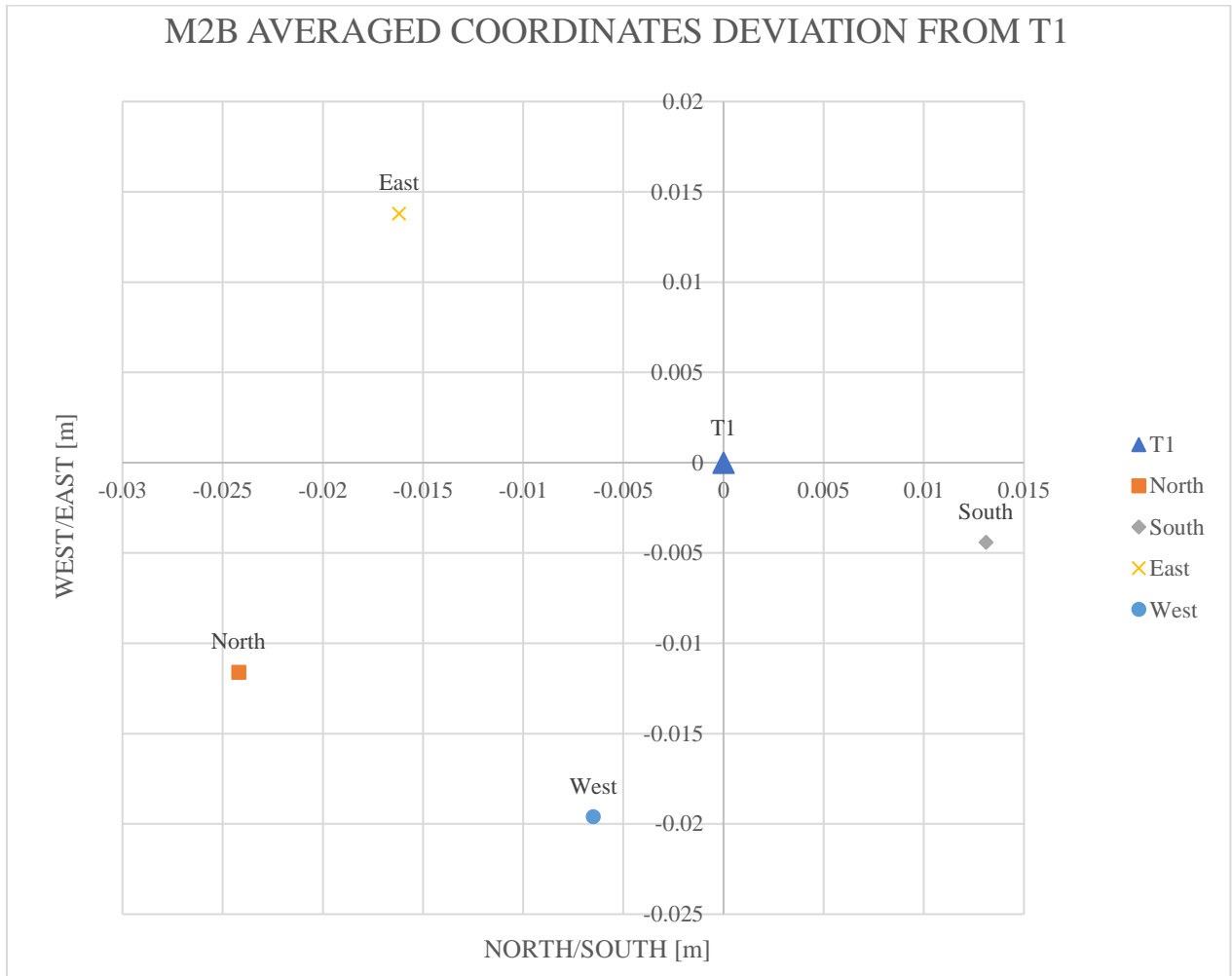


Figure 17 - M2B Averaged coordinates deviation from benchmark *T1*.

Figure 18 depicts Table 11 visually, showing how all observation sets have some observations relatively close to the benchmark. Interestingly the precision deviates the most for the north-tilted values, and to a lesser extent the east-tilted. The deviation for precision is dominant with regards to the north and eastern tilted observations.

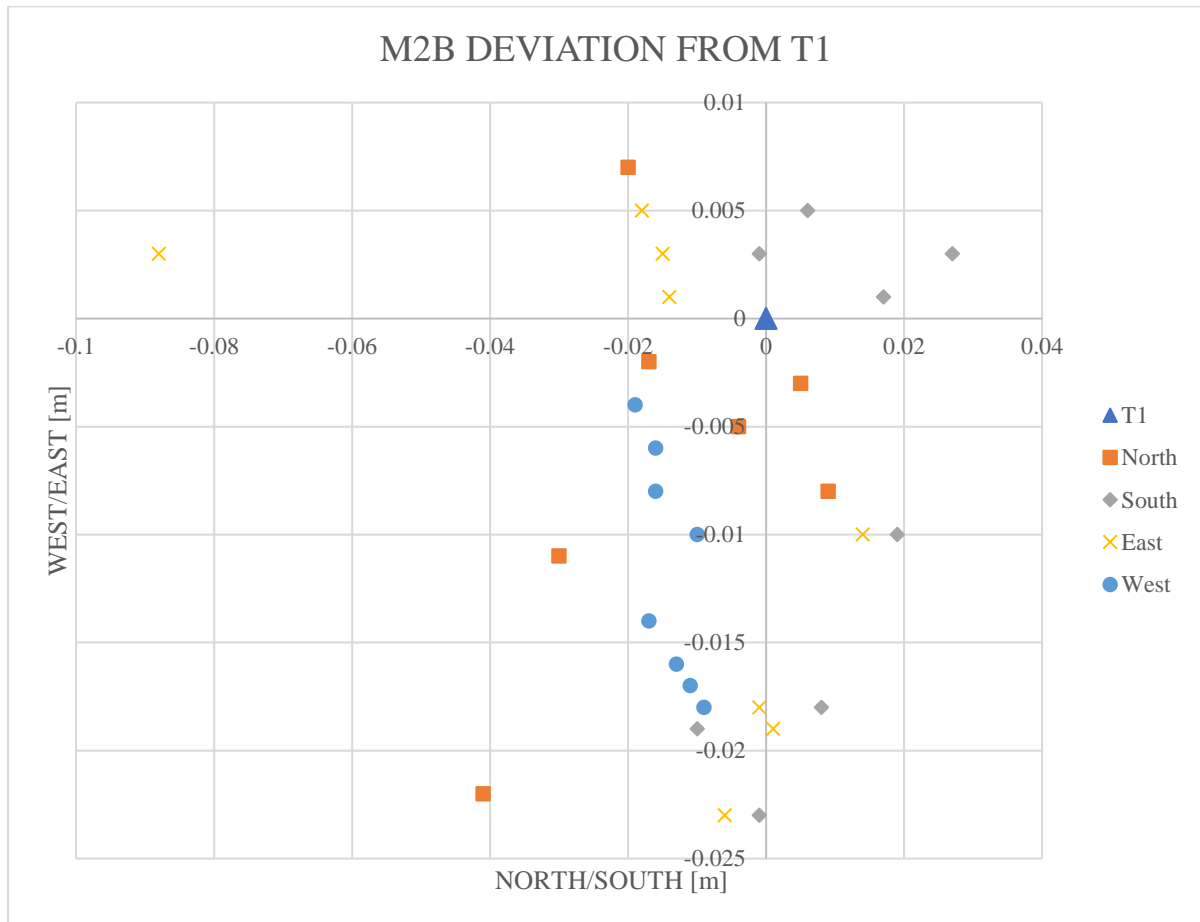


Figure 18 - M2B Deviation from the benchmark T1.

4.4 Method 3 – Building corners

The benchmark for corners 1, 2 and 3 were measured with the Leica MS60 total station and achieved a standard deviation of 6 millimetres or less on the horizontal plane.

Table 12 - M3A The benchmarks and standard deviations (U) for Corners 1, 2 and 3.

| POINT | N [m] | E [m] | H [m] | U(N) [m] | U(E) [m] | U(H) [m] |
|--------------|------------------------|------------------------|------------------------|---------------------------|---------------------------|---------------------------|
| B1 | 6 740 472.870 | 591 497.248 | 183.212 | 0.003 | 0.004 | 0.003 |
| B2 | 6 740 455.136 | 591 476.076 | 183.225 | 0.004 | 0.003 | 0.003 |
| B3 | 6 740 469.980 | 591 463.159 | 183.217 | 0.004 | 0.004 | 0.003 |

4.4.2 Receiver A

A gross error search was performed for the dataset where two observations from corner 1 and one from corner 2 were removed. The gross error search revealed none for corner 3.

Table 13 shows the standard deviations for the corner observations along with the mean coordinates. Corner 3 has the largest uncertainty in the northing and easting and corner 2 with the largest uncertainty in height.

Table 13 - M3A mean coordinates and standard deviation (U) for Northing(N), Easting(E), Height(H), and horizontal plane(2D).

| POINT | N [m] | E [m] | H [m] | U(N) [m] | U(E) [m] | U(H) [m] | U(2D) [m] |
|--------------|------------------------|------------------------|------------------------|---------------------------|---------------------------|---------------------------|----------------------------|
| C1 | 6 740 472.773 | 591 497.173 | 183.220 | 0.024 | 0.027 | 0.057 | 0.036 |
| C2 | 6 740 455.046 | 591 476.165 | 183.270 | 0.043 | 0.047 | 0.106 | 0.064 |
| C3 | 6 740 470.028 | 591 463.123 | 183.162 | 0.078 | 0.061 | 0.071 | 0.100 |

Comparing Table 14 with Table 13, it seems while corner 3 was the least precise of the measurements, it is also the most accurate with the lowest uncertainty in both the northing and easting.

Table 14 - M3A Average size of deviation (D) from benchmark T1 and RMS for Northing(N), Easting(E), Height(H) and horizontal plane(2D).

| POINT | D(N) [m] | D(E) [m] | D(H) [m] | D(2D) [m] | RMS(N) [m] | RMS(E) [m] | RMS(H) [m] | RMS(2D) [m] |
|-------|-------------|-------------|-------------|--------------|---------------|---------------|---------------|----------------|
| C1 | -0.091 | -0.112 | -0.015 | 0.144 | 0.094 | 0.115 | 0.055 | 0.148 |
| C2 | -0.081 | 0.104 | 0.014 | 0.132 | 0.091 | 0.113 | 0.101 | 0.145 |
| C3 | 0.048 | -0.036 | -0.055 | 0.060 | 0.089 | 0.069 | 0.087 | 0.112 |

Figure 19 shows all the corners' points average deviations from their respective benchmarks in one chart. The reason for corner 3 having a higher variation within observations is visualized clearly, including having a higher accuracy.

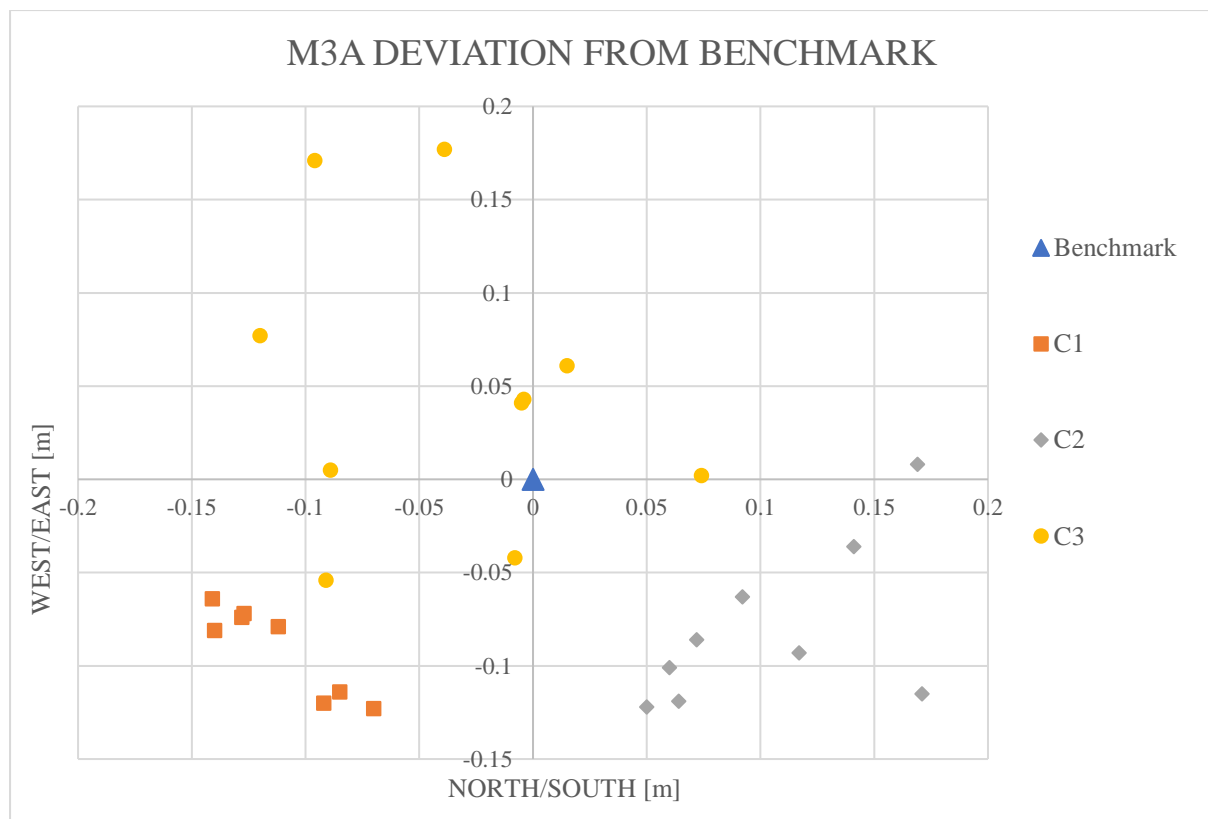


Figure 19 – M3A The deviations for all corners and observations from their respective benchmarks.

4.4.3 Receiver B

A gross error search revealed multiple gross errors. Corner 1 had a single gross error within the dataset for both the 15° observation and the 30° observations. Corner 2 error search revealed and removed a single observation for the 15° and none for 30°. Corner 3 had a single observation for the 15 and two for the 30° observation removed.

Table 15 shows the 15° observations at corner 2 had the overall largest uncertainty in precision. For the most part, the observations at both 15 and 30° were similar, there is no indication the 30° observations were considerably less precise than the 15° observations.

Table 15 - M3B Mean coordinates and standard deviation (U) for Northing(N), Easting(E), Height(H), and horizontal plane(2D).

| POINT | N [m] | E [m] | H [m] | U(N) [m] | U(E) [m] | U(H) [m] | U(2D) [m] |
|-------|---------------|-------------|----------|-------------|-------------|-------------|--------------|
| C1 15 | 6 740 472.895 | 591 497.260 | 183.223 | 0.027 | 0.023 | 0.030 | 0.036 |
| C1 30 | 6 740 472.900 | 591 497.282 | 183.245 | 0.054 | 0.044 | 0.020 | 0.070 |
| C2 15 | 6 740 455.113 | 591 476.050 | 183.215 | 0.071 | 0.051 | 0.071 | 0.088 |
| C2 30 | 6 740 455.160 | 591 476.090 | 183.197 | 0.047 | 0.046 | 0.026 | 0.066 |
| C3 15 | 6 740 469.982 | 591 463.142 | 183.212 | 0.025 | 0.017 | 0.032 | 0.032 |
| C3 30 | 6 740 470.004 | 591 463.156 | 183.202 | 0.021 | 0.021 | 0.054 | 0.030 |

Table 16, shows the average deviation from the benchmark and RMS does not indicate that there is any great advantage with either of the two tilt degrees. In corner 1, the closest to the benchmark seems to have been the 30° observation and in corner 3, the 15° observation seems to be the closest to the benchmark. Corner 2 seems to be the corner with the largest uncertainty in accuracy.

Table 16 - M3B Average size of deviation (D) from benchmark TI and RMS for Northing(N), Easting(E), Height(H) and horizontal plane(2D).

| POINT | D(N) [m] | D(E) [m] | D(H) [m] | D(2D) [m] | RMS(N) [m] | RMS(E) [m] | RMS(H) [m] | RMS(2D) [m] |
|-------|-------------|-------------|-------------|--------------|---------------|---------------|---------------|----------------|
| C1 15 | -0.021 | -0.014 | -0.014 | 0.025 | 0.033 | 0.026 | 0.031 | 0.042 |
| C1 30 | -0.029 | -0.001 | -0.002 | 0.029 | 0.059 | 0.041 | 0.019 | 0.072 |
| C2 15 | 0.023 | 0.026 | -0.003 | 0.034 | 0.071 | 0.055 | 0.054 | 0.090 |
| C2 30 | -0.024 | -0.014 | 0.015 | 0.028 | 0.051 | 0.046 | 0.051 | 0.069 |
| C3 15 | -0.007 | 0.002 | 0.025 | 0.007 | 0.026 | 0.016 | 0.039 | 0.031 |
| C3 30 | -0.021 | 0.016 | 0.032 | 0.026 | 0.029 | 0.025 | 0.060 | 0.038 |

In Figure 20 for the majority of observations at all the corners are within 5 cm. And as shown in Table 15 and Table 16, corner 2 seems to have the largest spread and deviation from the benchmark in the observation series.

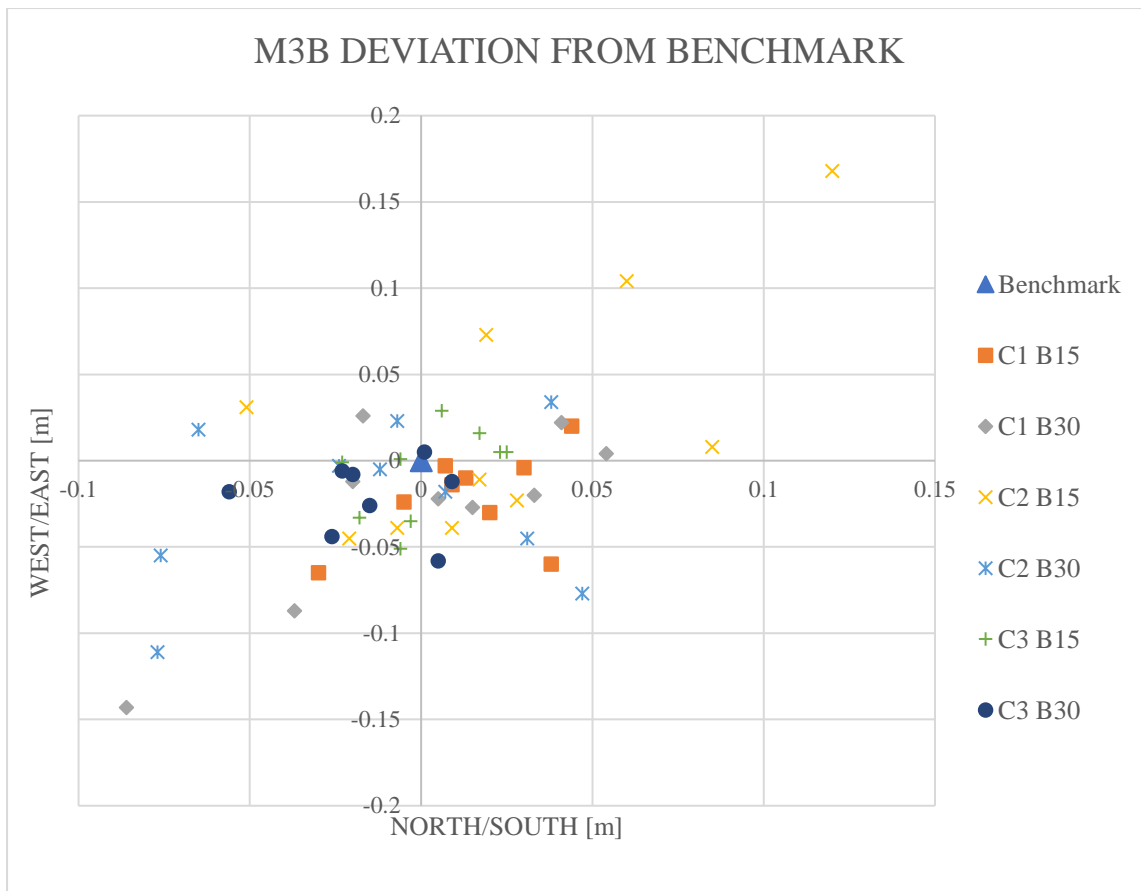


Figure 20 - M3B The deviation for all the corners and observations from their respective benchmarks.

4.5 Method 4 – Manhole

For the observations in the manhole, only receiver B was used as we no longer had receiver A.

The first three sessions were removed because of large gross errors. The measuring case was challenging and performing the observations needed practice. The sixth session faced some of the same issues as the first three, as it was the first session on the second day of measuring.

Table 17 shows the largest difference between all the measured points and gives an indication of the largest difference that would be likely in a similar case without any gross errors. The largest difference is the east coordinate.

Table 17 - M4 Minimum and Maximum values for coordinates and heights with the difference.

| Min North [m] | Max North [m] | Min East [m] | Max East [m] | Min Height [m] | Max Height [m] |
|-----------------------------|---------------|----------------------------|--------------|------------------------------|----------------|
| 6740513.169 | 6740513.252 | 591526.766 | 591526.897 | 180.907 | 180.997 |
| Difference North [m] | | Difference East [m] | | Difference Height [m] | |
| 0.083 | | 0.131 m | | 0.09 m | |

Table 18 shows the standard deviation for the series, it is expected that these would be rather low as all the observations in the series would have been correlated. It is also of note, that although some series have a larger standard deviation, there is nothing that indicates one of the series might contain gross errors. Interesting here that there does not seem to be any significant difference in the uncertainty between the north and east.

Table 18 - M4 Standard deviations for each observation series.

| | U(N) [m] | U(E) [m] | U(H) [m] |
|------------|----------|----------|----------|
| K1 | 0.007 | 0.010 | 0.014 |
| K2 | 0.007 | 0.007 | 0.006 |
| K3 | 0.008 | 0.012 | 0.004 |
| K4 | 0.009 | 0.004 | 0.010 |
| K5 | 0.007 | 0.007 | 0.009 |
| K6 | 0.005 | 0.005 | 0.005 |
| K7 | 0.004 | 0.006 | 0.009 |
| K8 | 0.006 | 0.004 | 0.008 |
| K9 | 0.006 | 0.008 | 0.014 |
| K10 | 0.007 | 0.005 | 0.004 |
| K11 | 0.005 | 0.012 | 0.007 |
| K12 | 0.012 | 0.009 | 0.008 |
| K13 | 0.006 | 0.010 | 0.006 |
| K14 | 0.007 | 0.007 | 0.004 |
| K15 | 0.011 | 0.012 | 0.005 |

Table 19 shows the standard deviations for all observations in M4. As in Table 17, the east coordinate has the largest uncertainty and, unlike in Table 18, there seems to be a larger uncertainty in the east when looking at all the observations.

Table 19 - M4 Standard deviation for all the observations.

| | U(N) [m] | U(E) [m] | U(H) [m] | U(2D) [m] |
|------------|-------------|-------------|-------------|--------------|
| All Series | 0.017 | 0.031 | 0.015 | 0.035 |

Figure 21 presents the observation series compared to an averaged point from all observations. This shows some groupings of the different series. However, most of the observations are spread out and deviate from each other.

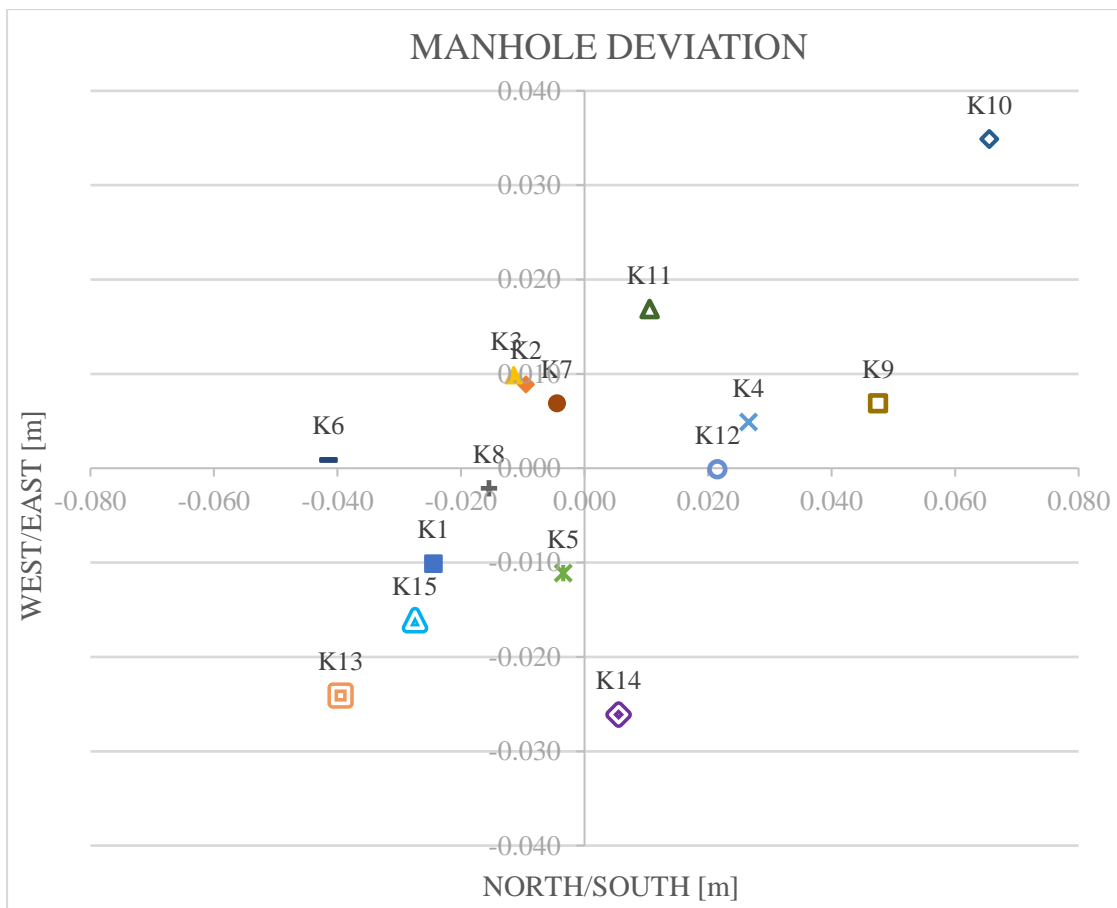


Figure 21 - M4 Manhole observations series compared to an averaged point from the observations.

5 Discussion

5.1 Considerations

Deciding to use ETPOS in concert with static observations to generate our benchmarks was predominantly based the bachelor course. ETPOS is not the standard for defining new benchmarks. Deciding to use this was due to it having the best absolute coordinates we have achieved through our bachelor course.

Defining benchmarks across the campus with high quality absolute positions was important to explore small deviations within measurements. Benchmarks on the building corners were defined with a total station which had done a free station to three or more of our newly defined benchmarks.

The rooftop point *TI* was defined by conducting three separate observations of three-hour sessions. Defining the *TI* was extra important as it was the benchmark for the measurements with presumably the highest accuracy and least deviation.

For all methods we chose to have handheld measurements as this was the most realistic. Handheld measurements will have variation in angle of rod tilt. The methods and where they were performed do have an impact on the results achieved. Method 1 and 2 were performed on a rooftop where there is likely multipath-related disturbance due to air vents, and after conducting the observations a strong magnetic force was found. While the magnetic force was consistent on the rooftop, neither receiver A, nor B reacted to it as an error source.

Receiver A

Receiver A was likely affected in method 1 and 2 by the magnetic force near the fence on the rooftop. This magnetic disturbance was equal on all measurement days and seemed to be included in the calibration process. The precision of the measurements themselves did not indicate a large source of error from this.

Receiver A had significantly large deviations from the coordinates of *TI*. The observations were done over several days, calibrations were done twice daily and the precision for the observations was consistent. After performing several tests, we concluded that the error likely stems from magnetic disturbances which the receiver itself does not notice. Using a regular handheld compass on the point we measured, indicated an incorrect north-direction of roughly 25° towards the west.

Comparing the 2D RMS of the corner observations in method 3 with the 2D RMS at 15° in method 1 and with the 2D RMS of the cardinal directions in method 3, is another indication that what we thought was an ideal place to measure for a benchmark was a problematic location.

Receiver B

The receiver requires movement to activate the tilt-compensation properly. When the receiver is held still over time, the compensation deviates more and more over until it deactivates the tilt-compensation (Myslivec, 2021).

5.2 Observation results

5.2.1 M1 Varying degrees of tilt

Receiver A

The results from M1 indicate that the observations are affected by a systematic error which increases with tilt. As observations were done over several days with multiple calibrations, a high precision indicates that something was consistently off about the measuring conditions, the equipment or how the equipment was handled. The observations seem to be quite precise, but they move further from the reference point as the tilt increases. That is the deviation from the reference point increases as tilt increases. The rod was tilted towards the south-western direction, but the tilt-function mirrors the measured points lying south-east from *TI*.

Due to large deviations from *TI* indicated in the data processing phase, some simple tests were performed to see if there were any gross errors involved. The height of the rod was correct seeing as the observation with a 0° tilt gave correct height and expected accuracy. The second test was to see if the tilt-function works correctly, and it does somewhat compensate for the tilt. Taking the receiver's position along the horizontal plane in comparison to the benchmark has significantly different values than measured. With the tilt-compensation turned off, the deviations would on average be roughly twice as large as observed.

Receiver B

The average deviation shows a steady decrease in accuracy with increased tilt from 10°. Regarding municipal requirements, the equipment would function for most purposes considering the level of accuracy required. Commercial accuracy requirements are stricter, and not always met when using the tilt-compensation. Interesting to note how the accuracy is

greater for the observation with a 10°-tilt than the levelled observation without tilt-compensation. It is possible that the tilt-function is more accurate than the physical level on the rod and observer levelling.

The observations seem to indicate that the easting value has a significantly greater variation with increased tilt. Interesting to look at how the tilt-compensation corrects for more than 94% of the horizontal distance from measured point to receiver. Using the equipment does require some considerations as gross errors did appear within the observations.

5.2.2 M2 Cardinal directions

Receiver A

The results from M2A show that a tilt towards the east leads to a significant decline in precision of northing values. Regardless of decreased precision, it is slightly more accurate than the north-tilted observations relative to the benchmark. Interesting to see how the deviation of observations accuracy is larger for the coordinates (northing/easting) that are perpendicular to the axis of tilt. The north/south axis has a higher deviation from the benchmark along the easting coordinate and vice versa for the east/west axis.

The placement of the averaged coordinates (Figure 15) do show the points being rotated roughly 100° anti-clockwise. Why the measured points seemed to have been rotated around the benchmark requires further studies. Deviation from the benchmark is similar for all cardinal direction observations that have been inclined towards. As the deviation is of a similar size, there is likely a systematic error. The observations were done over several days and calibrated twice or more daily. The placements of the observations in relation to the benchmark can indicate that the receiver has trouble finding geographic north, requires further studies.

Receiver B

The variation within the dataset in M2B show a clear difference between north and east in comparison to south and west. When tilted to the north, the easting has the higher variation. Whereas the variation of the easting when tilted to the east is also the most effected.

The stated accuracy of the receiver itself when tilted to such a degree is 24.5 mm along the horizontal plane, which all but the east-tilted observations are within. The observations tilted to the north, west and south do hold an accuracy of less than the RA. The observation tilted to the east is not quite as accurate with RMS of 35 mm. The easting is the main problem for all

the observations. Municipal accuracy requirements in terms of horizontal and height accuracy are met (Indre Østfold Kommune, 2021). The commercial requirement is also achieved for the South and West inclined observations, though not for the north and east tilted (Powel, 2018).

5.2.3 M3 Building corners

Receiver A

Although the observations at corner 3 had a larger variation within the dataset, that also resulted in a higher accuracy compared to the benchmark. When measuring corner 3, the receiver signalled a warning for magnetic disturbances if it was closer than 15° to the door. Considering how the observation grouped at corner 1 and 2, it seems likely the spread in the observations is indicative of magnetic disturbances.

Differing cardinal directions tilt observations (C1 south, C2 south-west, C3 north-west) do not seem to affect either the northing or easting significantly.

Receiver B

Comparing the 15° and 30° tilt, there is no significant difference in the accuracy or precision of the observations. Indicating anything between at least 15°-30° would give similar results, which is in line with the findings of Myslivec (Myslivec, 2021) which concludes tilt up to 45° can be used for most surveying purposes.

For receiver B, corner 3 is the corner with the least deviations. The deviations in northing and easting are equal on the corners and do not seem to have been affected by the tilt directions to any significant degrees.

5.2.4 M4 Manhole

Evaluating the repeatability of the observations is interesting because looking purely at the standard deviation, it would indicate the equipment is quite precise. Looking at the maximum and minimum difference, indicates you might get large deviation between two observations without any gross errors in the observation series. There are a lot of variables in this case and when doing similar observations, the user should be aware of the chance for a large deviation between two observations.

When following Kartverkets standard for RTK GNSS observations (Kartverket, 2009) there are two methods. Either two observations with a time separation of 45 minutes or three

observations with 15 minutes time separation. Based on our results a maximum difference of 13 cm between two observations even without any gross errors could be expected and must be considered when choosing the observation procedure.

6 Conclusion and future studies

6.1 Conclusion

This study set out to investigate the accuracy and precision of tilt-compensated GNSS-receivers. The tests involved ideal and challenging observation environments and the results thereof.

While receiver A is precise in all three dimensions, only the height values are within the expected accuracy. The accuracy along the horizontal plane is lower than expected for surveying purposes, with an RMS between 0.112-0.230m. The reason for accuracy of the horizontal plane being below the expected value requires further research. Tilting in different cardinal directions gave a larger deviation from the benchmark along the axis perpendicular to the axis of tilt. While the rod was tilted towards north or south the easting deviated most from the benchmark, whereas east and west tilted observations had the largest deviation in the northing. Precision of the observations was weakest for the easting, except for the south tilted measurements.

Receiver B met the achieved positional uncertainty with varied tilt required for both municipal and most commercial requirements. The cardinal directions did affect the precision and accuracy to some extent, the deviation being either equal or greater in the easting for both precision and accuracy. The largest deviation was 0.031 m in precision and 0.033 in accuracy in easting for measurement tilted to the east.

Using receiver B in a challenging measuring environment gave results which indicate the degree of “challenging” needs to be considered. The results from the corners varied from a RMS of 0.031-0.090m and standard deviation of 0.030-0.088m. A greater degree of tilt resulted in the greater degree of uncertainty. The increased tilt in corner 2, in contrast, resulted in a more accurate measurement. This can indicate that certain locations may benefit or even rely on increased tilt to reduce obstructions. The precision of method 4 indicated it is within the requirements of the municipal and commercial surveyors.

We recommend that, when using tilt compensated GNSS equipment must be considered when deciding on how much to tilt the GNSS receiver. While a lower tilt angle in general is preferred, there might be some situations where increasing the tilt would be beneficial or even required based on local restrictions.

6.2 Future studies

A likely consequence of the receiver accepting satellites below the cut-off, is that cardinal directional biases are likely to influence positional uncertainty. The DOP value of the receiver likely becomes skewed as it is only being influenced by a portion of the satellite constellation. Consequently, testing to see what the receiver computes to be its actual attitude would be an interesting research subject.

Comparing the work of Myslivec (2021) and Almstedt and Peterson (2019) with our results when measuring at 0° , whereas Myslivec recommends turning on the tilt compensator for observations at 0° Almstedt & Peterson recommend turning it off. These contrasting recommendations warrant further investigation.

References

Almstedt, Å. and Peterson, N. (2019) *Lägesosäkerhet vid nätverks-RTK-mätning med inbyggd lutningskompensator: en undersökning av Leica GS18 T*. Available at: <http://urn.kb.se/resolve?urn=urn:nbn:se:hig:diva-30505> (Accessed: 2 February 2021).

Amin, A.-L. and Watkins, G. (2018) *How sustainable infrastructure can help us fight climate change*, *World Economic Forum*. Available at: <https://www.weforum.org/agenda/2018/11/building-sustainable-infrastructure-matters-climate-change/> (Accessed: 12 May 2021).

Berber, M. and Arslan, N. (2013) 'Network RTK: A case study in Florida', *Measurement*, 46(8), pp. 2798–2806. doi: 10.1016/j.measurement.2013.04.078.

Carlson (2021) *Carlson Software*. Available at: <https://www.carlsonsw.com/product/brx7-gnss-receiver/> (Accessed: 13 May 2021).

CHCNAV (2021) *i90: IMU-RTK GNSS Smart Antenna | CHCNAV*. Available at: <https://www.chcnav.com/product-detail/i90-imu+++rtk-gnss> (Accessed: 13 May 2021).

Comnav (2021) *T300 Plus solution_ComNav Technology Ltd*. Available at: http://www.comnavtech.com/t300p_solution.html (Accessed: 13 May 2021).

Hi-Target (2021) *iRTK4 GNSS RTK System, Hi-Target Surveying Instrument Co.Ltd*. Available at: <https://en.hi-target.com.cn/irtk4-gnss-rtk-system/> (Accessed: 13 May 2021).

Hong, S. *et al.* (2005) 'Observability of error States in GPS/INS integration', *Vehicular Technology, IEEE Transactions on*, 54, pp. 731–743. doi: 10.1109/TVT.2004.841540.

Horizon (2021) *Horizon D6+ GNSS RTK Receiver, Horizon SG*. Available at: <https://horizon.sg/horizon-d6-gnss-rtk-receiver/> (Accessed: 13 May 2021).

Indre Østfold Kommune (2021) 'Innmåling og dokumentasjon av VA-ledningsnett'. Indre Østfold Kommune. Available at: https://www.io.kommune.no/_f/p1/i7bf1a364-5b5e-4ea0-b145-680301d95c8b/innmaling-og-dokumentasjon-av-va-ledningsnett-003.pdf (Accessed: 17 February 2021).

Kartverket (2009) ‘Satellittbasert Posisjonsbestemmelse’. Available at: <https://www.kartverket.no/globalassets/geodataarbeid/standardisering/standarder/standarder-geografisk-informasjon/satellittbasert-posisjonsbestemmelse-2.1-standarder-geografisk-informasjon.pdf> (Accessed: 17 February 2021).

Kartverket (2011) ‘Stedfesting av matrikkelenhets og raderettsgrenser’. Available at: <https://kartverket.no/globalassets/geodataarbeid/standardisering/standarder/standarder-geografisk-informasjon/stedfesting-av-matrikkelenhets-og-raderettsgrenser-2011-10-03-standarder-geografisk-informasjon.pdf> (Accessed: 17 February 2021).

Kartverket (2015) ‘Geodatastandarden’. Available at: <https://www.kartverket.no/globalassets/geodataarbeid/standardisering/standarder/standarder-geografisk-informasjon/geodatakvalitet-1.0-standarder-geografisk-informasjon.pdf> (Accessed: 15 March 2021).

Kartverket (2020a) *Få veiledning om CPOS, Kartverket.no*. Available at: <https://kartverket.no/til-lands/posisjon/hva-er-cpos> (Accessed: 16 February 2021).

Kartverket (2020b) *Få veiledning om ETPOS, Kartverket.no*. Available at: <https://kartverket.no/til-lands/posisjon/hva-er-etpos> (Accessed: 8 March 2021).

Kartverket (2021) *Brukerveiledning posisjonstjenester, Kartverket.no*. Available at: <https://kartverket.no/til-lands/posisjon/brukerveiledning-posisjonstjenester> (Accessed: 17 February 2021).

Kjerstad, N. (2021) ‘Treghetsnavigasjon’. snl.no. Available at: <https://snl.no/treghetsnavigasjon>.

Lachapelle, G. and Alves, P. (2002) ‘Multiple Reference Station Approach: Overview and Current Research’, *Journal of Global Positioning Systems*, 1(2), pp. 133–136.

Leica (2021) *Leica GS18 T GNSS RTK Rover*. Available at: <https://leica-geosystems.com/products/gnss-systems/smart-antennas/leica-gs18-t> (Accessed: 13 May 2021).

Leick, A., Rapoport, L. and Tatarnikov, D. (2015) *GPS Satellite Surveying*. 4th edition. Hoboken, New Jersey: John Wiley & Sons.

Luo, X. *et al.* (2018) ‘High-Precision RTK Positioning with Calibration-Free Tilt Compensation’. Available at: https://www.researchgate.net/publication/325022922_High-Precision_RTK_Positioning_with_Calibration-Free_Tilt_Compensation.

Myslivec, J. (2021) *Testing the accuracy and usability of the GNSS receiver Leica GS18 I*. České vysoké učení technické v Praze. Vypočetní a informační centrum. Available at: <https://dspace.cvut.cz/handle/10467/93179> (Accessed: 20 April 2021).

Norkart (2021) *GISLINE*. Norkart.

Odolinski, R. (2012) ‘Temporal correlation for network RTK positioning’, *GPS Solutions*, 16(2), pp. 147–155. doi: 10.1007/s10291-011-0213-0.

Ohlsson, K. (2014) *Studie av mätosäkerhet och tidskorrelationer vid mätning med nätverks-RTK i SWEPOS 35 km-nät*. Available at: https://www.lantmateriet.se/contentassets/85bfe36b48a04d4d8d652ed790c309d0/2014_5.pdf.

Powel (2018) *VA - Inmålingsinstruks, Powel.no*. Available at: <https://volueinfrastructure.com/va-instruks> (Accessed: 13 May 2021).

SatLab (2021) *SL900 GNSS Receiver – SatLab – Global Satellite Positioning Solutions*. Available at: https://www.satlab.com.se/product_uri/satlab-sl900-gnss-receiver/ (Accessed: 13 May 2021).

SBG Systems (2020) *IMU - Inertial Measurement Unit, IMU - Inertial Measurement Unit*. Available at: <https://www.sbg-systems.com/inertial-measurement-unit-imu-sensor/> (Accessed: 16 May 2021).

Skogseth, T. and Norberg, D. (2014) *Grunnleggende landmåling*. 3rd edn. Gyldendal Undervisning.

Tersus GNSS (2021) *Oscar GNSS Receiver | Extreme RTK with Tilt Compensation*. Available at: https://www.tersus-gnss.com/product/oscar_gnss_receiver (Accessed: 13 May 2021).

Topcon (2021) *HiPer VR, Topcon Positioning Systems, Inc*. Available at: <https://www.topconpositioning.com/gnss-and-network-solutions/integrated-gnss-receivers/hiper-vr> (Accessed: 13 May 2021).

Trimble (2021) *Trimble R12i GNSS System*. Available at: <https://r12i.trimble.com/> (Accessed: 13 May 2021).

United Nations (2021) *Goal 9*. Available at: <https://sdgs.un.org/goals/goal9> (Accessed: 12 May 2021).

Van Sickle, J. (2021a) *The Ionospheric Effect*. Available at: <https://www.e-education.psu.edu/geog862/node/1715> (Accessed: 9 March 2021).

Van Sickle, J. (2021b) *The Space Segment: Dilution of Precision*. Available at: <https://www.e-education.psu.edu/geog862/node/1771> (Accessed: 9 March 2021).

Zimmerman, R. and Faris, C. (2010) 'Chapter 4: Infrastructure impacts and adaptation challenges', *Annals of the New York Academy of Sciences*, 1196(1), pp. 63–86. doi: <https://doi.org/10.1111/j.1749-6632.2009.05318.x>.

Appendix

Appendix 1 – Benchmark reports and adjustment equalizations

Appendix 2 – Mission_planning.pdf

